# TECTONOTHERMAL EVOLUTION OF THE NORTHERN MINTO BLOCK, SUPERIOR PROVINCE, QUEBEC, CANADA

JOHN A. PERCIVAL[§] AND THOMAS SKULSKI[§]

*Geological Survey of Canada, 601 Booth Street, Ottawa, Ontario K1A 0E8, Canada*

## ABSTRACT

Previously considered one of Earth's largest granulite terranes, the Minto block, in northern Quebec, consists dominantly of granitic rocks with sparse supracrustal remnants that record low-pressure, high-temperature metamorphism to the amphibolite and granulite facies at *ca.* 2.7 Ga. Much of the region is underlain by plutonic rocks, including igneous charnockitic bodies, that provide little evidence of metamorphism. In contrast, pelitic assemblages in low-grade greenstone belts and their higher-grade shoulders define four metamorphic zones: 1) sub-staurolite-grade slates, found only in the Duquet belt, 2) staurolite – andalusite – sillimanite – garnet-zone schists, present in all belts, 3) marginal garnet – sillimanite ± kyanite migmatites, and 4) garnet – sillimanite ± cordierite and garnet – orthopyroxene granulites, as enclaves within plutonic units. A prograde low-pressure, high-temperature regional facies-series is defined by andalusite – sillimanite assemblages, thermobarometric analyses that indicate peak conditions ranging from 3 kbar, 560°C to 8.4 kbar, 840°C, and short segments of anticlockwise P–T trajectories preserved in two of the lowest-grade areas. Kyanite occurs in migmatites in the vicinity of a *ca.* 2.81 Ga shear zone bounding two distinct supracrustal assemblages and marks an earlier Barrovian event. All belts are polydeformed, with a common, broadly synmetamorphic, NNW-striking, steep foliation and down-dip lineation related to regional-scale $F_2$ folds. Distributed late-metamorphic dip-slip shear appears responsible in some areas for cross-strike juxtaposition of low- and high-grade metamorphic zones. Older, generally poorly preserved $D_1$ deformation, recognized in several belts, may represent accretionary structures. Variably developed younger deformation includes NNW dextral transcurrent brittle–ductile shear zones ($S_3$), variably developed east-trending $F_4$ folds, and WNW-striking pseudotachylite zones. U–Pb monazite ages of 2702 Ma date high-grade metamorphism of a pelitic granulite, crystallization of two diatexites, and staurolite-zone metamorphism in one schist. Together with similar zircon ages of crust-derived granites, these data point to a major collisional orogeny at this time. Older titanite (2748–2765 Ma) indicates areas that escaped >650°C metamorphism during the 2.7 Ga event. Younger monazite occurs in a migmatite-grade rock (2688, 2672 Ma) and staurolite-zone schists (2679–2642, 2648, 2637, and 2642–2628 Ma), similar to titanite ages in greenstones (2643–2550 Ma) and $^{40}Ar/^{39}Ar$ hornblende ages (2.64–2.56 Ga). These post-peak metamorphic ages in the greenstone belts based on monazite and titanite are attributed to hydrothermal growth from fluids channeled along permeable zones; they may reflect late reheating events observed throughout the Superior Province as leucogranitic magmatism, metamorphism in the deep crust, and mineral growth in shear zones.

*Keywords*: greenstone belts, granulite, amphibolite, Archean, U–Pb ages, monazite, zircon, P–T conditions, geothermobarometry, tectonic models, Superior Province, Quebec.

## SOMMAIRE

Le socle de Minto, dans le nord du Québec, considéré antérieurement comme un des plus vastes terrains de roches transformées aux conditions du faciès granulite sur terre, est surtout un collage de roches granitiques avec des restes épars de roches supracrustales qui témoignent d'un métamorphisme à faible pression et à température élevée, aux conditions du faciès amphibolite et granulite il y a environ 2.7 Ga. La plupart de la région expose des roches plutoniques, y compris des charnockites ignées, qui ne manifestent que très peu de signes d'une recristallisation métamorphique. En revanche, les assemblages pélitiques des ceintures de roches vertes, métamorphisées à faible température, et leurs bordures à un degré de métamorphisme plus élevé, définissent quatre zones métamorphiques: 1) ardoises, degré de métamorphisme inférieur au sous-faciès à staurotide, limitées à la ceinture de Duquet, 2) schistes à staurotide – andalousite – sillimanite – grenat, présents dans chaque ceinture, 3) migmatites à grenat – sillimanite ± kyanite, en bordure, et 4) granulites à grenat – sillimanite ± cordiérite et grenat – orthopyroxène, en enclaves dans les unités plutoniques. L'identification d'une séquence de faciès typique de faible pression et de température élevée repose sur la présence d'assemblages à andalousite – sillimanite, les analyses thermobarométriques indiquant des conditions maximales allant de 3 kbar, 560°C à 8.4 kbar, 840°C, et de courts intervalles de tracés P–T contre le sens de l'horloge qui sont préservés dans deux des régions où le degré de métamorphisme est le plus faible. On trouve la kyanite près d'une zone de cisaillement datée à environ 2.81 Ga entre deux assemblages supracrustaux distincts; ce serait le vestige d'un événement barrovien antérieur. Toutes les

---

§    *E-mail addresses*: joperciv@nrcan.gc.ca, tskulski@nrcan.gc.ca

ceintures sont polydéformées, ayant en commun une foliation généralement synmétamorphique, orientée vers le NNO et à pendage abrupt, avec linéations parallèles au pendage liées au plis $F_2$, développés à l'échelle régionale. Un cisaillement tardif parallèle au pendage semble responsable de la juxtaposition transversale et locale de zones métamorphique de faible et de forte intensité. Nous avons trouvé des exemples d'une déformation $D_1$, généralement mal préservée, dans plusieurs ceintures, et il pourrait s'agir de structures d'accrétion. Parmi les signes d'une déformation plus tardive, inégalement développée, seraient les zones de cisaillement dextres NNO à caractère cassant ou ductile ($S_3$), des plis $F_4$ variablement développés et orientés vers l'est, des zones de pseudotachylite à orientation ONO. Des âges U–Pb obtenues sur monazite, 2702 Ma, définissent l'épisode de métamorphisme d'une granulite pélitique, la cristallisation de deux diatexites, et le métamorphisme d'un schiste dans la zone de la staurolite. Avec les âges semblables déterminés sur zircon des granites dérivés dans la croûte, ces données indiquent une orogenèse majeure liée à une collision dans cet intervalle. Les âges plus anciens déterminés sur la titanite (2748–2765 Ma) caractérisent les endroits ayant échappé au métamorphisme à >650°C au cours de l'événement de 2.7 Ga. Des âges plus jeunes déterminés sur la monazite caractérisent une roche migmatitique (2688, 2672 Ma) et des schistes à staurolite (2679–2642, 2648, 2637, et 2642–2628 Ma), et ressemblent aux âges déterminés sur la titanite des roches vertes (2643–2550 Ma) et aux âges $^{40}Ar/^{39}Ar$ sur la hornblende (2.64–2.56 Ga). Ces dates postérieures à la culmination métamorphique, établies sur la monazite et la titanite des ceintures de roches vertes, seraient dues à une croissance hydrothermale de ces accessoires à partir d'une phase fluide migrant le long de zones perméables. Cette croissance pourrait résulter d'événements causant un réchauffement tardif observé partout dans la province du Supérieur, par exemple la mise en place de leucogranites, un métamorphisme de la croûte inférieure, et une croissance de minéraux accessoires dans des zones de cisaillement.

## INTRODUCTION

Metamorphic rocks house a wealth of information, concerning for example minerals and structures developed during burial and exhumation, as well as ages of deposition, crystallization, metamorphism and cooling. Resolving these events may be particularly challenging in polydeformed regions where strain markers, metamorphic assemblages, barometers, thermometers and chronometers may record non-coincident points on P–T–t paths. Valid interpretations of the tectonic significance of regional metamorphism depend on multiple field- and laboratory-derived constraints.

Models for the tectonic evolution of Precambrian terranes have relied to a large degree on Phanerozoic analogues. That uniformitarian principles can be applied indiscriminately to crust formed as long ago as the Archean has been challenged on the basis of dissimilarities in the geological record (*e.g.,* Goodwin 1996, Hamilton 1998), and has rejuvenated an alternative tectonic model for the Archean involving vertical additions to the crust and associated diapirism. It is useful in the context of deciphering the Earth's early evolution to test these competing models of the Archean tectonic regime with observations from Archean cratons.

As a natural laboratory, the Archean Superior Province of the Canadian Shield offers the benefits of large size, in which the scale of tectonic features may be assessed, a range of exposure levels and metamorphic grade, and a rapidly expanding geoscience database (*e.g.,* Card 1990, Williams *et al.* 1992, Stott 1997). In this paper, we contribute quantitative P–T–t information on the Minto block of northeastern Superior Province, previously known only as a large ($2.5 \times 10^6$ km²)

high-grade region (Stevenson 1968, Percival *et al.* 1992). Our aim is to provide a tectonometamorphic framework for the evolution of the region within the broad-scale context of the Superior Province. Characterized by low-pressure, high-temperature facies series at a range of exposure levels, the Minto block provides insight into the driving mechanisms of metamorphism and the relationship between metamorphism and magmatism, key elements in tectonic models of orogens of all ages.

## GEOLOGICAL SETTING

Located in the northeastern Superior Province of Quebec, the Minto block (Fig. 1) represents part of a Mesoarchean (3.0–2.8 Ga) protocraton that was assembled and reworked by magmatic and tectonic processes between 2.8 and 2.68 Ga (Percival *et al.* 1994, Stern *et al.* 1994). It is characterized by a prominent NNW structural grain that contrasts with the east–west alignment of subprovinces and structural fabrics in the southern Superior Province. The gradational, 200-km-wide transition zone occurs within the pluton-dominated Bienville Subprovince, suggesting that the structural transition is an Archean feature, intruded by the dominant 2.73–2.69 Ga suites of granitic rocks of the Bienville Subprovince (Skulski *et al.* 1998) and Minto block.

Whereas the northern Superior protocraton, including the North Caribou Terrane of Ontario (Fig. 1; Thurston *et al.* 1991) has Mesoarchean ancestry, many of the subprovinces of the southern Superior represent juvenile Neoarchean crust (Machado *et al.* 1986, Henry *et al.* 1998). In current tectonic models, the northern protocraton is considered a continental nucleus onto
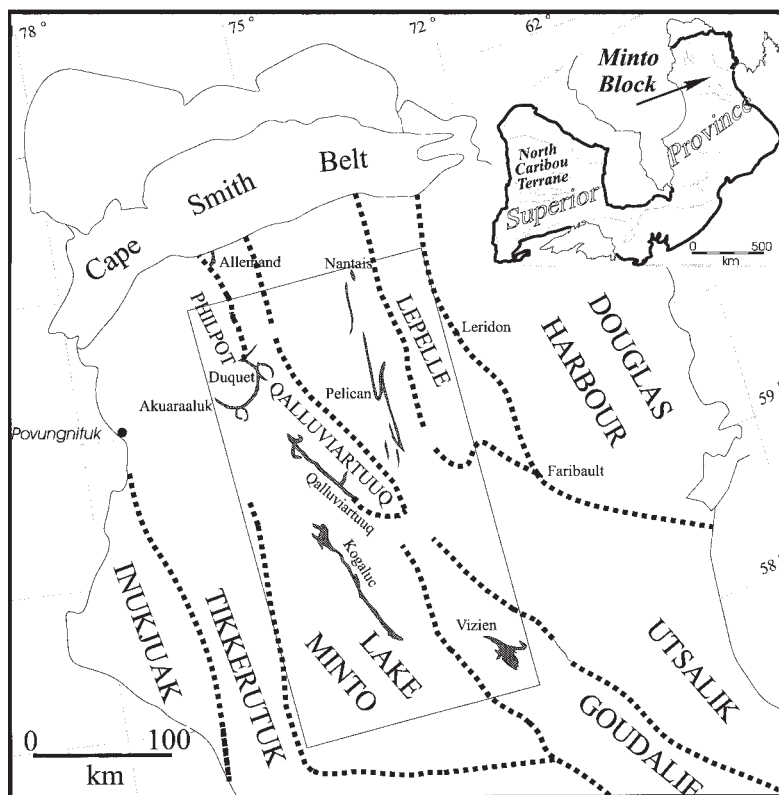
FIG. 1.   Regional domains of the Minto block, compiled from Percival & Card (1994), and Percival *et al.* (1995b, 1996b, 1997b) and extrapolations from aeromagnetic maps. Inset map shows location of the Minto block in the Superior Province.

which juvenile plateau and arc terranes were accreted at 2.71–2.69 Ga (Card 1990, Williams *et al.* 1992, Percival *et al.* 1994, Stott 1997). Prominent metasedimentary belts represent collisional flysch basins fed by tectonic highlands shedding arc-type detritus mixed with older sources (Davis *et al.* 1989, 1990, Corfu *et al.* 1995, Davis 1996).

Where it has been accurately dated, metamorphism in the middle to upper crust of the southern belts followed the main deformation by 10–30 m.y. For example, major deformation in the English River Subprovince occurred at *ca.* 2.70 Ga, whereas high-grade metamorphism affected the rocks in the range 2.69–2.68 Ga (Corfu *et al.* 1995). Deformation of similar age in the Wabigoon – Winnipeg River region was followed by greenschist- to amphibolite-facies metamorphism *ca.* 2.69 Ga (Menard *et al.* 1997). In the Quetico belt, polyphase deformation occurred prior to 2.68 Ga, and medium- to high-grade metamorphism took place *ca.* 2.67 Ga (Percival 1989), similar to constraints provided by the on-strike Ashuanipi complex

(Percival 1991, 1994). The main regional deformation in the Abitibi belt occurred prior to 2.69 Ga (Mortensen 1993, Corfu 1993), whereas the rocks experienced their greenschist-facies peak of metamorphism between 2.675 and 2.645 Ga (Powell *et al.* 1995a, b). Several conclusions may be drawn from these data: 1) individual subprovinces have distinct tectonothermal histories, 2) deformation and metamorphism proceeded in a general way from north to south, and 3) metamorphism occurred shortly after deformation in the southern Superior Province belts.

Northwesterly aeromagnetic trends in the Minto block of northern Quebec reflect domains of distinct geological and geophysical character. In general, the broad positive aeromagnetic anomalies correspond to relatively magnetic pyroxene-bearing granitic massifs, whereas the lows are occupied by belts of less magnetic supracrustal rocks and associated biotite- and hornblende-bearing granitic rocks (Pilkington & Percival 1999). Magnetic models indicate that the belts of supracrustal rocks have V-shaped keels up to 10 km

thick. Gravity anomalies mimic the long-wavelength magnetic pattern, with highs over granitic and granulitic massifs, and lows associated with supracrustal belts.

Geological characteristics of the domains have been explored through recent mapping and geochronology (Fig. 1; Percival & Card 1994, Skulski *et al.* 1996, Percival *et al.* 1997a), augmented by previous helicopter-based reconnaissance mapping (Stevenson 1968) and reconnaissance SHRIMP dating (Percival *et al.* 1998). These studies provide an image of the Minto block as the complex end-product of a series of orogenic events between 2.8 and 2.7 Ga (Percival & Skulski 1997). Scattered remnants of ancient (2.8–3 Ga) crust occur in the east, in the Goudalie and Douglas Harbour domains (Fig. 1), possibly representing an orogenic foreland during subsequent tectonic events. Supracrustal rocks, including associated ultramafic units and quartzites in the Faribault and Leridon belts (Percival *et al.* 1997a), may represent a platform rift-cover sequence similar to that described from the northwestern Superior Province (Thurston & Chivers 1990). Volcanic and associated rocks in the Qalluviartuuq domain of the north-central Minto block range in age from 2.84 to 2.77 Ga and have juvenile Nd isotopic signatures (Skulski *et al.* 1996) which, with pillows and other evidence of submarine deposition, suggest ocean-floor and arc settings. Intra-oceanic $D_1$ accretionary structures and associated metamorphism, recognized locally, are described below.

Development of a successor arc at *ca.* 2.775 Ga was followed by deposition of an unconformable sequence of conglomerate, greywacke and iron formation after 2748 Ma (Percival & Skulski 1998), possibly in a rifted arc setting. These sedimentary units are exposed mainly as high-grade schists and gneisses in the Lake Minto domain (Fig. 1). Calc-alkaline magmatism of 2730–2720 Ma age is widespread throughout the Minto block (Percival, Stern & Skulski, unpubl. data) and represents voluminous continental arc magmatism (Stern *et al.* 1994). In the east (Utsalik domain), Nd isotopic signatures of granodiorites indicate significant involvement of older crust, whereas in the west (Lake Minto domain), rocks of similar age and composition are relatively juvenile isotopically.

The western Minto block was reworked during a second major orogenic event at *ca.* 2.70 Ga. Effects included burial of *ca.* 2.72 Ga supracrustal rocks of the Vizien belt (Percival *et al.* 1993, Skulski & Percival 1996, Lin *et al.* 1996), low-P, high-T metamorphism (Bégin & Pattison 1994), formation of upright folds and shear zones, and emplacement of crust-derived granites and diatexites (Percival *et al.* 1992, Stern *et al.* 1994). Most of the information in this paper relates to the *ca.* 2.7 Ga event. The wide extent of high-grade metamorphic rocks exhumed from mid-crust levels supports a model of crustal thickening and metamorphism followed by isostatic rebound. Late east–west-trending cross-folds are responsible for some structural relief.

## ANALYTICAL METHODS

Electron-microprobe analyses were done on a Camebax instrument equipped with wavelength-dispersion spectrometers. We used an accelerating voltage of 15 kV, with specimen current varying from 10 to 30 nA, depending on the mineral species. Counting times varied from 10 to 30 seconds per element, for total count durations of ~100 s per spot. Standards included a variety of minerals, oxides and metals, and data reduction was performed on routines provided by Pouchou & Pichoir (1984). Analytical reproducibility is on the order of ±5% for most elements. Structural formulae were calculated using programs developed by G.J. Pringle. The extent of zoning was assessed through step traverses. Garnet with significant zoning occurs in sample 1139 and was mapped in one crystal on a 5 μm grid using 3-s count times.

Accessory minerals were extracted for geochronology using conventional crushing, heavy liquid and Frantz purification techniques. Zircon and monazite were hand-picked using an optical microscope, and the zircon was air-abraded following the method of Krogh (1982) prior to dissolution and analysis. U–Pb analytical procedures were summarized by Parrish *et al.* (1987), and the treatment of errors follows Roddick (1987), with regression analysis modified after York (1969). Isotopic data have been corrected for the measured U and Pb blanks, 0.3 pg and 2–31 pg, respectively.

Hand-picked hornblende separates intended for $^{40}Ar/^{39}Ar$ dating were loaded into aluminum foil packets and arranged in an aluminum can with flux monitor PP–20 hornblende, collected from the same quarry as (and identical to) HB3gr, with an apparent age of 1072 Ma (Roddick 1983). Samples were irradiated at the research reactor of McMaster University, with a resulting J-factor of approximately 0.0195 to 0.0198, with variation corrected by interpolation along the length of the can. Irradiated samples were split into 2–4 aliquots and heated separately using a 45 W Weck $CO_2$ surgical laser with a beam *ca.* 200 μm in diameter optically attenuated by 20×, and analyzed with a VG3600 gas-source mass spectrometer; data-collection protocols follow Villeneuve & MacIntyre (1997), and data reduction of individual aliquots follows Roddick (1988). Some of the data show the effects of "hot spots" that disrupt small gas-fractions derived from the higher-temperature parts of the gas-release spectra, likely the result of slightly heating previously unheated regions of the grain. Analytical results are available from Depository of Unpublished Data, CISTI, National Research Council, Ottawa, Ontario K1A 0S2, Canada. The data plots differ from conventional $^{40}Ar/^{39}Ar$ spectra in that data from individual aliquots are displayed in adjacent, alternately shaded regions of the gas-release spectra. Once reproducibility of individual spectra and plateau regions is established between aliquots, the data were combined

by integrating plateau portions. The error in J-factor (±0.5%, 1σ) is then applied to the final age quoted.

## TECHNIQUES OF GEOTHERMOBAROMETRY

In general, analyses were done on proximal garnet, biotite, pyroxene, cordierite and plagioclase grains separated by non-ferromagnesian minerals, in order to avoid potentially retrograde zones. Mineral compositions were used to calculate P–T conditions using a variety of equilibria and TWQ software (Berman 1988, 1991) updated to TWQ, version 2.02. Thermochemical parameters are taken from the internally consistent database of Berman & Aranovich (1996), which contains modifications relevant to this study for biotite, orthopyroxene and cordierite. For pelitic rocks, the garnet – biotite thermometer (Grt–Bt; abbreviations from Kretz 1983) and the grossular – anorthite – sillimanite – quartz barometer provide the most common P–T intersections.

Several samples contain the assemblage Grt–Bt–Pl–Qtz–Sil–Crd, allowing application and comparison of the Grt–Bt–Pl–Qtz–Sil and Grt–Crd–Sil–Qtz thermobarometers. For rocks of the granulite facies, mineral-core analyses yield similar P–T values using both systems, whereas for rims, Bt–Grt–Pl–Sil–Qtz gives pressures lower by 1–1.7 kbar than Grt–Crd–Sil–Qtz. In lower-grade rocks, both cores and rims yield lower (0.1–1.3 kbar) Grt–Crd–Sil–Qtz pressures and generally lower (up to 135°C) Grt–Crd temperatures.

An estimate of P–T errors for individual samples, taking account of the reproducibility of the electron-microprobe analyses and uncertainty in thermochemical parameters, is generally taken to be on the order of ±50°C, 1 kbar (Kohn & Spear 1991). Additional uncertainty is due to the possible effects of retrograde equilibration and other natural factors. This uncertainty may be assumed to be larger in the granulite facies than in lower-grade rocks owing to increased probability of retrograde Fe–Mg exchange at high temperature (Frost & Chacko 1989, Bégin & Pattison 1994).

## DISTRIBUTION AND GENERAL CHARACTER OF METAMORPHIC ZONES

Herd (1978) divided the Minto block into amphibolite, granulite and retrograde granulite facies on the basis of a re-examination of Stevenson's (1968) collection. However, much of the Minto block consists of plutonic rocks, which are not sensitive monitors of metamorphic grade. Hence definition of metamorphic zones depends on the sporadic presence of units with informative assemblages. Plutons include hornblende- and biotite-bearing and charnockitic (pyroxene-bearing) types, here referred to for convenience as "wet" and "dry" plutons, respectively. There is a spatial association between amphibolite-facies schists and "wet" plutons, and between granulite-facies gneisses and "dry" (charnockitic)

plutons. The relationship between plutonism and metamorphism is discussed in more detail below.

Four prograde regional metamorphic zones have been identified in the present study, primarily on the basis of assemblages developed in aluminous metasedimentary rocks (Fig. 2). The lowest grade, in the upper greenschist facies, occurs in a 5 × 10 km patch in the northern Duquet belt. There, delicate sedimentary structures are preserved in slaty rocks characterized by the assemblage chlorite – muscovite – biotite (Fig. 3). At higher grade, equivalent units contain spectacular porphyroblasts of andalusite and staurolite, suggesting grade control rather than unfavorable composition for the lower-grade assemblages. The amphibolite facies, defined by pelitic assemblages including staurolite and andalusite (Fig. 4), characterizes the main belts of supracrustal rock. On their flanks, in regions dominated by plutonic rocks, are upper-amphibolite-facies zones in which garnet- and sillimanite-bearing pelites are migmatitic. Large areas within the granulite facies consist largely of charnockitic plutonic units with sparse screens of migmatitic supracrustal rocks containing garnet – sillimanite ± cordierite or orthopyroxene-bearing assemblages (Percival *et al.* 1990).

Assemblages of the middle-amphibolite facies in rocks of pelitic (Table 1), mafic, ultramafic and altered compositions define low-P, high-T metamorphic conditions. P–T conditions are constrained on petrogenetic grids (Fig. 5) by textural relations in all belts for the prograde reactions:

andalusite = sillimanite [1],

and

staurolite = garnet + aluminosilicate
+ quartz + $H_2O$ [2]
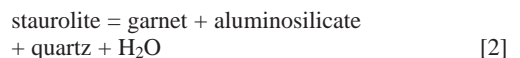
In the FMASH system, appropriate for these generally muscovite-free assemblages, these equilibria cross at approximately 3 kbar, 550°C (Carmichael 1978, Davidson *et al.* 1990).

Metamorphosed altered rocks yield cordierite–anthophyllite-bearing assemblages that also are sensitive monitors of grade in the amphibolite facies. Assemblages define P–T conditions on Spear's (1993) grid in the range 2.5–4 kbar, 550–600°C. Ultramafic units also are useful indicators of temperature in the amphibolite facies.

## BELTS OF AMPHIBOLITE-FACIES SUPRACRUSTAL ROCKS

Coherent packages of supracrustal rocks occur in isolated belts (greenstone belts), separated by along- or across-strike granitic massifs. Although there are common stratigraphic, structural and metamorphic elements among the belts, they are first described individually,

followed by a synthesis of the regional tectonometamorphic history. Precise correlation of lithological units, structural and metamorphic events is tenuous owing to the inability to date critical events. Thus correlations are based on common sequences of events and geometrical similarity.

### Vizien belt

The 40 by 10 km Vizien belt (Figs. 1, 2) consists of middle-amphibolite-facies rocks of volcanic and sedimentary origin. It has been divided into six fault-bounded lithotectonic panels with distinct internal
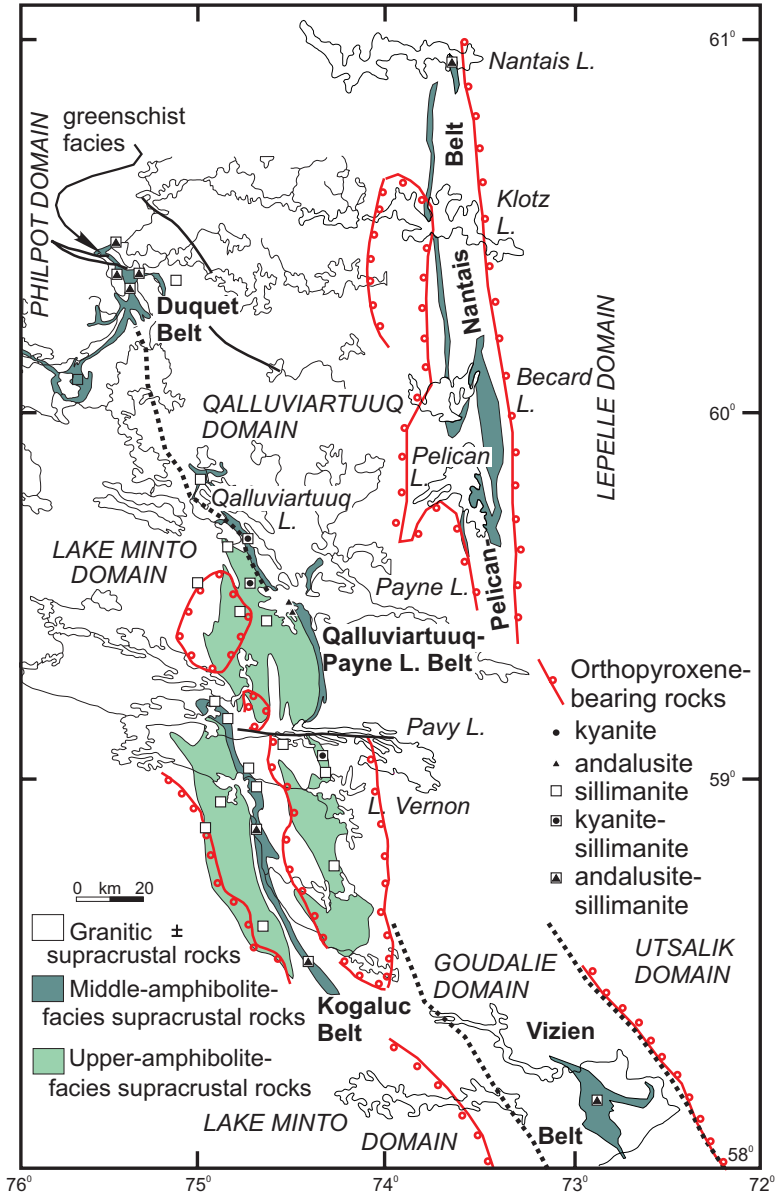


Fɪɢ. 2.    Metamorphic zones and major supracrustal belts of the north-central Minto block.

FIG. 3. Slaty cleavage in greenschist-facies metagreywacke, northern Duquet belt.
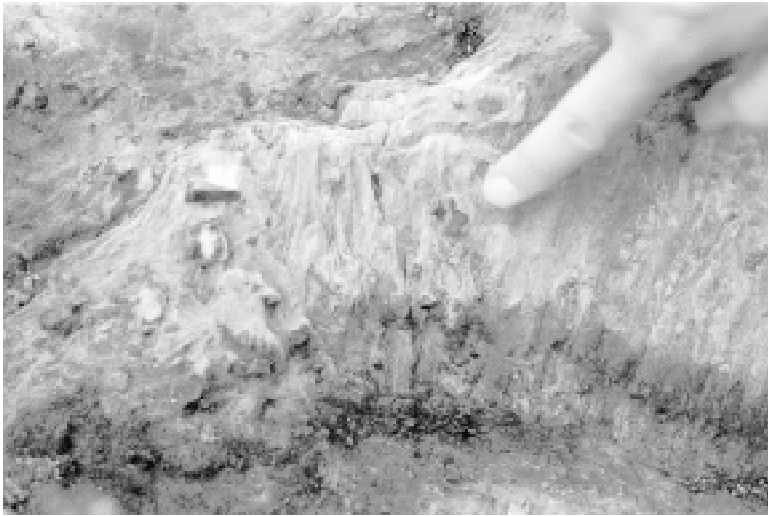


FIG. 4. Staurolite porphyroblasts in middle-amphibolite-facies pelitic schist, Payne Lake belt.

stratigraphy (Percival & Card 1992, Percival *et al.* 1993, Skulski *et al.* 1994, Lin *et al.* 1995).

The oldest supracrustal rocks comprise a sheet of mafic–ultramafic composition with basal serpentinite schist, overlain by peridotite, gabbro and basalt. A gabbro sill yielded concordant zircon with a $^{207}Pb/^{206}Pb$ age of 2786 ± 1 Ma (Skulski & Percival 1996). The sheet is in tectonic contact (Lin *et al.* 1996) with three distinct sequences: 1) A calc-alkaline volcanic arc sequence comprises mafic through felsic compositions. The basal unit consists of andesite and basalt with lenses of peridotite, iron formation and metamorphosed alteration zones (cordierite – anthophyllite – cummingtonite – tourmaline rocks). Overlying these are porphyritic andesite, dacite and rhyolite with a U/Pb zircon age of 2724 ± 1 Ma (Percival *et al.* 1992). 2) A second volcanic sequence consists of bimodal, probably subaerial, tholeiitic lavas and rare clastic sedimentary rocks

TABLE 1. SAMPLE LOCATIONS AND P-T RESULTS FROM NORTHERN MINTO BLOCK SAMPLES

| Sample | Easting[1] | Northing | Assemblage[2] | P–T$_1$ | | P–T$_2$ | | P–T$_3$ | P–T$_4$ |
|---|---|---|---|---|---|---|---|---|---|
| | | | | core | rim | core | rim | | |
| **Middle-amphibolite facies** | | | | | | | | | |
| Vizien PBAC92-2009 | 617710 | 6442175 | Grt-St-And-Sil-Bt-Qtz-Pl | 4.6, 635 | 3.8, 565 | | | | |
| PBAS94-274 | 615200 | 6441999 | Qtz-Pl-Bt-Mnz | | | | | | |
| Kogaluc SNB93-495 | 498330 | 6564425 | Grt-Sil-Bt-Qtz-Pl-Mnz | 4.8, 660 | 5.1, 660 | | | | |
| SNB93-428 | 505050 | 6559950 | Grt-St-And-Sil-Crd-Bt-Qtz-Pl-Ms | 6.5, 705 | 5.1, 650 | 5.3, 705 | 4.9, 660 | | |
| SNB93-401 | 504750 | 6560700 | Grt-Sil-Bt-Qtz-Pl | 5.7, 710 | 4.4, 605 | | | | |
| Payne PBA95-1139 | 526222 | 6593390 | Grt-St-And-Sil-Bt-Qtz-Pl-<u>Chl</u> | 3.0, 530 | 4.4, 585 | | | | |
| PBA95-1477 | 528000 | 6594000 | St-Bt-Pl-Qtz-Mnz | | | | | | |
| PBAS96-154 | 527350 | 6593725 | Bt-Pl-Ksp-Qtz-Zrn | | | | | | |
| PBAS96-1418 | 521000 | 6597850 | Bt-Pl-Qtz-Ttn | | | | | | |
| Qalluviartuuq PBA94-756 | 509065 | 6609634 | Grt-**St**-Sil-**Ky**-Bt-Qtz-Pl-Ms | 4.9, 665 | 3.6, 595 | | | | |
| PBA95-1064 | 498986 | 6627075 | Bt-Pl-Ksp-Qtz-Zrn | | | | | | |
| PBAS95-1421 | 498555 | 6630551 | Bt-Pl-Qtz-Ttn | | | | | | |
| PBAS95-1461 | 501871 | 6627075 | Hbl-Bt-Pl-Qtz-Ttn | | | | | | |
| PBAW94-290 | 498555 | 6630551 | Bt-Pl-Qtz-Ttn | | | | | | |
| QAN92 | 498650 | 6621700 | Hbl-Pl-Ttn | | | | | | |
| Duquet PBA95-1433 | 476229 | 6691922 | Grt-St-And-Sil-Bt-Qtz-Pl | 4.3, 600 | 3.3, 535 | | | | |
| PBAS95-1734 | 474410 | 6694450 | Grt-St-And-Sil-Bt-Qtz-Pl-Mnz | | | | | | |
| PBAS95-1738 | 463750 | 6724546 | Hbl-Bt-Pl-Qtz-Ttn | | | | | | |
| PBAS95-1739 | 485650 | 6699780 | Hbl-Bt-Pl-Qtz-Ttn | | | | | | |
| Nantais PBA95-1538 | 573570 | 6760500 | Grt-St-And-Bt-Qtz-Pl-Ms-Mnz-<u>Chl</u> | 2.7, 530 | 3.7, 550 | | | | |
| PBAS96-63A | 582557 | 6629977 | Ms-Bt-Pl-Qtz-Ttn | | | | | | |
| **Upper-amphibolite facies** | | | | | | | | | |
| PBA95-1517 | 514350 | 6605962 | Grt-Sil-Bt-Qtz-Pl | 5.8, 710 | 5.0, 640 | | | | |
| PBA94-691 | 519175 | 6588378 | Grt-Sil-Bt-Qtz-Pl | 7.4, 820 | 5.6, 710 | | | | |
| PBA94-618 | 510182 | 6601814 | Grt-Sil-**Ky**-Crd-Bt-Qtz-Pl-Mnz | 5.8, 720 | 4.3, 645 | 5.7, 690 | 5.0, 630 | | |
| PBA94-639 | 510914 | 6591082 | Grt-Sil-Crd-Bt-Qtz-Pl | 7.3, 810 | 6.3, 715 | 6.0, 675 | 5.2, 615 | | |
| PBA94-516a | 499056 | 6541840 | Grt-Sil-Bt-Qtz-Pl-Mnz | 3.3, 625 | 5.2, 630 | | | | |
| PBA95-1352 | 438971 | 6670698 | Grt-Sil-Bt-Qtz-Pl | 5.6, 710 | 5.8, 675 | | | | |
| **Granulite facies** | | | | | | | | | |
| PBA94-310 | 515990 | 6494967 | Grt-Sil-Crd-Bt-Qtz-Pl-Kfs | 7.8, 840 | 4.8, 725 | 7.0, 815 | 5.9, 710 | | |
| PBA94-281 | 500626 | 6517540 | Grt-Sil-Crd-Bt-Qtz-Pl | 5.6, 770 | 4.3, 645 | 6.3, 730 | 6.0, 695 | | |
| PBA94-255 | 533813 | 6542469 | Grt-Sil-Bt-Qtz-Pl-Mnz-Rt | 8.4, 805 | 2.4, 560 | | | | |
| PBA94-337 | 530073 | 6549255 | Grt-Sil-Crd-Bt-Qtz-Pl | 5.3, 700 | 3.8, 620 | 5.8, 690 | 4.8, 575 | | |
| PBA94-133 | 540218 | 6507833 | Grt-Opx-Qtz-Pl | | | | | 6.2, 730 | |
| PBA94-131b | 541141 | 6507135 | Grt-Cpx-Hbl-Qtz | | | | | | 6.2, 740 |
| PBAS94-132 | 533700 | 6506000 | Opx-Cpx-Hbl-Pl | | | | | | |
| PBA94-069 | 535818 | 6519703 | Grt-Opx-Cpx-Hbl-Pl-Qtz | | | | | 5.2, 630 | 7.2, 580 |
| PBAS96-149 | 583750 | 6620100 | Grt-Opx-Bt-Pl-Ksp-Qtz-Mnz | | | | | | |

[1] All UTM coordinates refer to grid zone 18

[2] Mineral abbreviations after Kretz (1983). Bold text indicates relict phase; underlined text indicates secondary phase

P – T$_1$: garnet – biotite thermometer; GASP barometer. P quoted in kbar, T in °C.

P – T$_2$: garnet – biotite thermometer; cordierite = garnet + sillimanite barometer

P – T$_3$: garnet – orthopyroxene thermometer; garnet – plagioclase – orthopyroxene – quartz barometer

P – T$_4$: garnet – clinopyroxene thermometer; garnet – plagioclase – clinopyroxene – quartz barometer

(Percival *et al.* 1993, Skulski *et al.* 1994). The estimated age of a rhyolite is 2722$^{+15}_{-8}$ Ma; inherited grains up to 2793 ± 8 Ma are present. 3) A basement-cover sequence consists of tonalitic basement (2940 ± 5 Ma) and an unconformable coarse clastic sedimentary sequence. Boulder conglomerates contain mainly tonalitic clasts; one graphic granite cobble provided single-crystal (zircon) $^{207}$Pb/$^{206}$Pb ages of 2718 to >3000 Ma, thus indicating sediment deposition after 2718 Ma (Percival *et al.* 1993). Above the conglomerate are psammitic and pelitic schists, locally intruded by gabbro sills (2700 ± 3 Ma) and overlain by basaltic andesite and siliceous high-magnesium basalt (Skulski & Percival 1996). The uppermost unit is a *mélange* containing angular and rounded fragments of variably deformed gabbro, serpentinite and rare chert in a serpentinitic matrix (Percival *et al.* 1993, Skulski & Percival 1996).
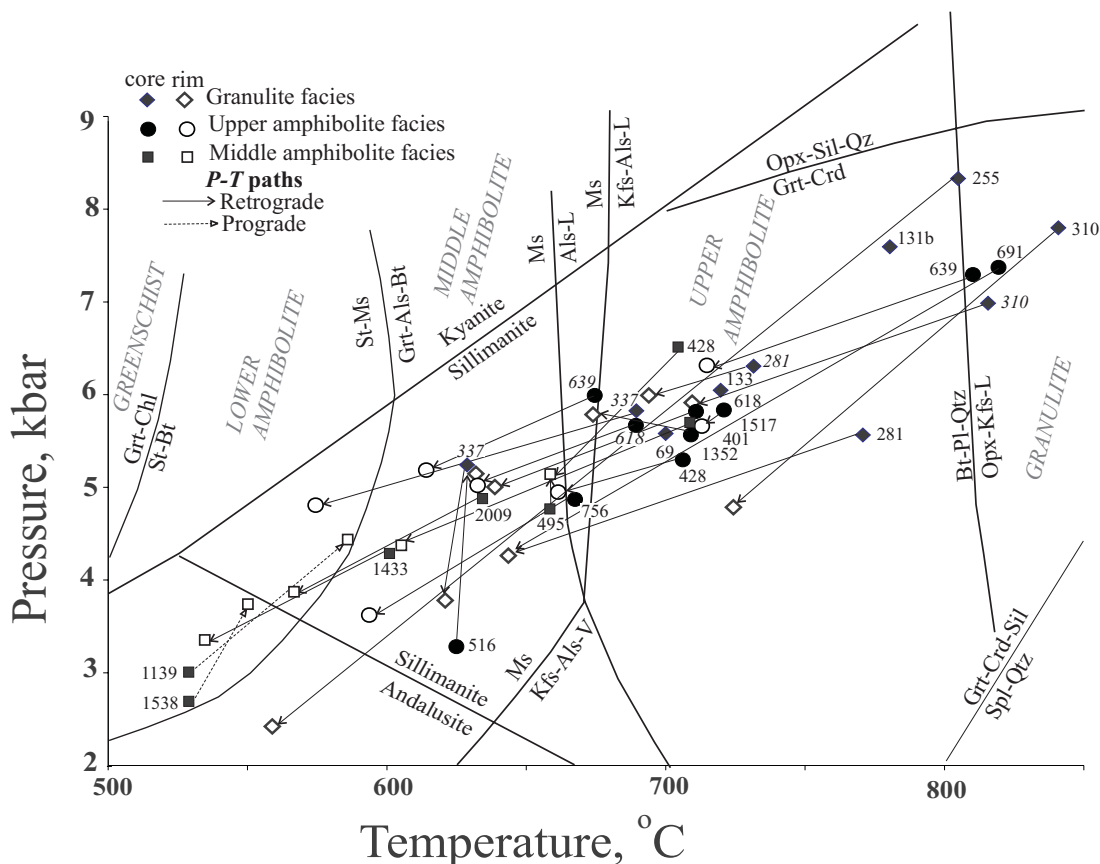
Fig. 5. P–T petrogenetic grid for pelites showing the position of equilibria relevant to rocks of the amphibolite and granulite facies in the Minto block (modified after Davidson *et al.* 1990, Carrington 1995). P–T points are those reported in Table 1.

The Vizien belt records a complex structural history (Percival & Card 1992, Percival *et al.* 1993, Skulski *et al.* 1994, Lin *et al.* 1996), including five phases of ductile deformation and late brittle faulting (Lin *et al.* 1995). The oldest ($D_1$) involved formation of a *mélange* as the mafic–ultramafic sheet was thrust onto the younger basement-cover sequence. The $D_2$ event imposed a penetrative shear fabric ($S_2$) during amalgamation of the discrete lithotectonic packages. $D_3$ resulted in open to tight folds of $S_2$ and panel boundaries, and was followed by the development of open $D_4$ cross folds, and later ($D_5$) dextral transcurrent tectonic mixing in an eastern boundary zone. $D_1$ deformation postdates deposition of the cover sequence (<2718 Ma), and $S_2$ is cut by peraluminous granitic pegmatite with $^{207}Pb/^{206}Pb$ monazite ages of 2620 to 2693 ± 1 Ma (T. Skulski, unpubl. data).

The grade of metamorphism is expressed in a wide variety of bulk-rock compositions that consistently indicate amphibolite-facies conditions. Metaperidotites contain relict igneous forsterite ($Fo_{80–87}$; 0.5 wt% NiO) and spinel, as well as metamorphic minerals defining

reaction [3], which occurs at approximately 550°C in the 3–4 kbar pressure range (Evans 1977):

serpentine (antigorite) = forsterite + talc + $H_2O$ [3]
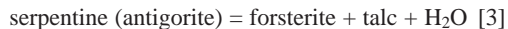
Assemblages in altered bulk-compositions include anthophyllite, cordierite, cummingtonite, magnesian clinochlore, and rare staurolite (Schwarz 1992); they define metamorphic conditions in the range 550–580°C, 3–4 kbar on the basis of Spear's (1993) grid. In pelite from the basement-cover sequence (2009), relict staurolite and andalusite occur in association with the peak assemblage garnet – biotite – plagioclase – sillimanite, suggesting operation of the reaction:

staurolite + quartz = garnet
+ aluminosilicate + $H_2O$ [4].

In detail, determination of whether the reaction commenced in the andalusite field and continued in the sillimanite field, or took place in the presence of metastable

## TABLE 2. REPRESENTATIVE COMPOSITIONS* OF GARNET

| sample | G2009 | G401 | G428 | G495 | G1139 | G756 | G1433 | 1538 | G1517 | G691 | G618 | G639 | G516 | G1352 | G310 | G281 | G255 | G337 | G133 | G131 | G069 |
|--------|-------|------|------|------|-------|------|-------|------|-------|------|------|------|------|-------|------|------|------|------|------|------|------|
| | core | core | core | core | core | core | core | core | core | core | core | core | core | core | core | core | core | core | core | core | core |
| SiO2 | 38.28 | 35.58 | 36.4 | 36.39 | 35.75 | 36.96 | 36.33 | 35.42 | 36.45 | 36.81 | 37.31 | 37.29 | 36.53 | 35.76 | 37.41 | 37 | 37.89 | 37.22 | 36.63 | 37.07 | 36.85 |
| TiO2 | 0 | 0.03 | 0.05 | 0.04 | 0.07 | 0.01 | 0 | 0 | 0 | 0 | 0.04 | 0 | 0 | 0 | 0 | 0.1 | 0.08 | 0.02 | 0.08 | 0.18 | 0 |
| Al2O3 | 20.2 | 20.67 | 21 | 21.05 | 20.78 | 21.3 | 21 | 20.89 | 20.79 | 21.44 | 21.43 | 21.94 | 20.92 | 21.25 | 21.46 | 21.47 | 22.06 | 21.51 | 21.09 | 20.81 | 21.17 |
| Cr2O3 | 0.09 | 0.05 | 0 | 0.07 | 0.05 | 0.04 | 0.05 | 0.02 | 0.01 | 0.03 | 0.01 | 0.01 | 0.06 | 0.08 | 0.11 | 0.1 | 0 | 0.06 | 0.03 | 0.03 | 0.02 |
| FeO | 33.25 | 33.24 | 34.5 | 33.87 | 32.57 | 34.7 | 32.88 | 37.22 | 35.73 | 33.29 | 34.42 | 33.17 | 36.05 | 33.5 | 32.54 | 32.13 | 28.55 | 34.59 | 31.06 | 29.72 | 29.51 |
| MgO | 2.76 | 4.03 | 4.23 | 3.59 | 2.6 | 4.54 | 3.17 | 1.34 | 3.46 | 6.33 | 5.4 | 6.32 | 4.14 | 4.08 | 7.38 | 6.23 | 8.9 | 5.54 | 3.27 | 2.99 | 3.31 |
| MnO | 2.92 | 2.95 | 2.21 | 3.87 | 4.83 | 1.69 | 4.14 | 3.41 | 1.16 | 0.42 | 0.82 | 0.47 | 1.42 | 3.04 | 0.5 | 0.59 | 0.68 | 0.87 | 2.3 | 1.57 | 1.67 |
| CaO | 1.45 | 1.11 | 1.17 | 1.13 | 1.7 | 1.2 | 1.48 | 1.44 | 1.03 | 1.11 | 1.11 | 1.28 | 0.93 | 0.98 | 0.89 | 1.05 | 1.47 | 1.07 | 5.25 | 7.54 | 7.06 |
| TOTAL | 98.95 | 97.71 | 99.64 | 100.01 | 98.52 | 100.65 | 99.18 | 100 | 98.72 | 99.7 | 100.72 | 100.7 | 100.32 | 98.95 | 100.58 | 98.76 | 99.8 | 101.13 | 99.94 | 100.11 | 99.82 |
| Grs | 0.0353 | 0.0314 | 0.0328 | 0.0317 | 0.0488 | 0.334 | 0.0422 | 0.041 | 0.0296 | 0.0303 | 0.0305 | 0.0352 | 0.0259 | 0.0275 | 0.0238 | 0.0297 | 0.0398 | 0.0294 | 0.145 | 0.2086 | 0.1959 |
| Prp | 0.1173 | 0.1603 | 0.1647 | 0.1402 | 0.1038 | 0.1757 | 0.1258 | 0.053 | 0.1383 | 0.2403 | 0.2062 | 0.2421 | 0.1603 | 0.1592 | 0.2745 | 0.2448 | 0.3352 | 0.2115 | 0.1256 | 0.1151 | 0.1278 |
| Alm | 0.7844 | 0.7416 | 0.7538 | 0.7422 | 0.7379 | 0.7538 | 0.7386 | 0.831 | 0.8058 | 0.7204 | 0.7455 | 0.7124 | 0.7826 | 0.7458 | 0.6911 | 0.7123 | 0.6104 | 0.7403 | 0.6792 | 0.6421 | 0.6396 |
| Sps | 0.063 | 0.0667 | 0.0487 | 0.0859 | 0.1096 | 0.0372 | 0.0934 | 0.076 | 0.0263 | 0.0091 | 0.0178 | 0.0102 | 0.0312 | 0.0674 | 0.0106 | 0.0132 | 0.0146 | 0.0189 | 0.0502 | 0.0343 | 0.0366 |

| sample | G2009 | G401 | G428 | G495 | G1139 | G756 | G1433 | 1538 | G1517 | G691 | G618 | G639 | G516 | G1352 | G310 | G281 | G255 | G337 | G133 | G131 | G069 |
|--------|-------|------|------|------|-------|------|-------|------|-------|------|------|------|------|-------|------|------|------|------|------|------|------|
| | rim | rim | rim | rim | rim | rim | rim | rim | rim | rim | rim | rim | rim | rim | rim | rim | rim | rim | rim | rim | rim |
| SiO2 | 38.45 | 36.51 | 36.44 | 36.51 | 36.6 | 36.82 | 36.64 | 35.51 | 36.47 | 37.34 | 37.2 | 37.25 | 36.7 | 36.01 | 37.32 | 37.25 | 36.31 | 36.88 | 37.06 | 36.94 | 37.07 |
| TiO2 | 0.04 | 0 | 0 | 0 | 0.05 | 0 | 0 | 0 | 0.02 | 0 | 0 | 0 | 0 | 0.05 | 0.01 | 0.04 | 0.06 | 0 | 0 | 0 | 0.02 |
| Al2O3 | 20.28 | 21 | 20.97 | 21 | 20.68 | 21.07 | 20.82 | 20.68 | 20.96 | 21.35 | 21.57 | 21.71 | 21.11 | 21.18 | 21.35 | 23.57 | 21.23 | 21.61 | 20.97 | 20.77 | 20.89 |
| Cr2O3 | 0 | 0.07 | 0 | 0.04 | 0.07 | 0.09 | 0.04 | 0.02 | 0.05 | 0.04 | 0.04 | 0.02 | 0.02 | 0.07 | 0.04 | 0.04 | 0.02 | 0.06 | 0.07 | 0.05 | 0.04 |
| FeO | 34.62 | 34.46 | 34.01 | 33.62 | 35.21 | 35.7 | 33.33 | 38.82 | 36.61 | 35.54 | 35.23 | 34.96 | 35 | 34.08 | 34.61 | 32.46 | 34.49 | 34.62 | 29.6 | 29.44 | 30.39 |
| MgO | 2.28 | 2.99 | 4 | 3.52 | 3.44 | 3.6 | 2.71 | 1.42 | 2.79 | 4.92 | 4.29 | 4.99 | 4.09 | 3.57 | 5.68 | 5.83 | 4.2 | 5.1 | 3.07 | 2.78 | 2.9 |
| MnO | 2.74 | 3.09 | 2.44 | 3.47 | 0.96 | 1.74 | 4.57 | 0.69 | 1.29 | 0.63 | 0.89 | 0.51 | 1.29 | 2.73 | 0.45 | 0.47 | 1.39 | 0.93 | 2.04 | 1.44 | 1.54 |
| CaO | 1.28 | 1.13 | 1.06 | 1.2 | 1.83 | 1.19 | 1.68 | 1.79 | 1.16 | 1.18 | 1.11 | 1.48 | 1.53 | 1.24 | 0.84 | 0.93 | 1.05 | 1.08 | 7.3 | 7.82 | 7.34 |
| TOTAL | 99.69 | 99.25 | 98.92 | 99.36 | 98.95 | 100.39 | 99.93 | 99.17 | 99.44 | 101.22 | 100.42 | 101.14 | 99.95 | 99.14 | 100.51 | 100.59 | 98.9 | 100.52 | 100.38 | 99.46 | 100.46 |
| Grs | 0.0381 | 0.0326 | 0.0302 | 0.0342 | 0.0522 | 0.0333 | 0.0446 | 0.051 | 0.0333 | 0.0322 | 0.0313 | 0.041 | 0.0416 | 0.0351 | 0.0231 | 0.0268 | 0.0299 | 0.0301 | 0.2012 | 0.2184 | 0.2021 |
| Prp | 0.0943 | 0.1201 | 0.1585 | 0.1396 | 0.1366 | 0.1402 | 0.1001 | 0.056 | 0.1116 | 0.187 | 0.1685 | 0.1922 | 0.1549 | 0.1407 | 0.2169 | 0.2334 | 0.1663 | 0.169 | 0.1177 | 0.108 | 0.1111 |
| Alm | 0.8033 | 0.7767 | 0.7563 | 0.748 | 0.7895 | 0.788 | 0.7594 | 0.877 | 0.8257 | 0.7672 | 0.7803 | 0.7556 | 0.7758 | 0.763 | 0.7503 | 0.7291 | 0.7726 | 0.7824 | 0.6387 | 0.6418 | 0.6532 |
| Sps | 0.0644 | 0.0705 | 0.055 | 0.0782 | 0.0217 | 0.0385 | 0.0959 | 0.016 | 0.0293 | 0.0136 | 0.0199 | 0.0112 | 0.0278 | 0.0611 | 0.0098 | 0.0107 | 0.0313 | 0.0185 | 0.0444 | 0.0318 | 0.0335 |

Compositions expressed as oxides in wt.%. * Electron-microprobe data.

## TABLE 3. REPRESENTATIVE COMPOSITIONS* OF BIOTITE

| Sample | B2009 | B401 | B428 | B495 | B1139 | B756 | B1433 | B1538 | B1517 | B691 | B618 | B639 | B516 | B1352 | B310 | B281 | B255 | B337 |
|--------|-------|------|------|------|-------|------|-------|-------|-------|------|------|------|------|-------|------|------|------|------|
| | core | core | core | core | core | core | core | core | core | core | core | core | core | core | core | core | core | core |
| SiO2 | 36.02 | 33.07 | 34.47 | 34.33 | 34.87 | 35.34 | 34.21 | 28.65 | 33.43 | 34.67 | 34.88 | 35.22 | 34.33 | 33.72 | 34.83 | 34.42 | 36.07 | 34.83 |
| Al2O3 | 18.74 | 18.84 | 19.61 | 18.85 | 19.1 | 18.98 | 20.05 | 19.88 | 18.89 | 18.7 | 18.05 | 18.75 | 18.6 | 18.53 | 17.54 | 17.05 | 16.76 | 19.31 |
| TiO2 | 1.73 | 1.7 | 1.34 | 1.67 | 1.54 | 2.06 | 1.47 | 1.6 | 1.91 | 3.39 | 2.44 | 3.41 | 1.88 | 3.14 | 4.56 | 5.29 | 4.3 | 3.84 |
| Cr2O3 | 0.14 | 0.06 | 0.24 | 0.04 | 0.12 | 0.08 | 0.06 | 0.06 | 0.2 | 0.06 | 0.18 | 0.12 | 0.04 | 0.13 | 0.19 | 0.2 | 0.05 | 0.16 |
| FeO | 19.6 | 19.25 | 18.25 | 18.66 | 17.05 | 17.15 | 17.58 | 27.66 | 20.6 | 17.34 | 16.92 | 15.1 | 17.49 | 19.13 | 16.77 | 16.35 | 13.1 | 15.22 |
| MnO | 0 | 0.24 | 0.07 | 0.19 | 0.1 | 0.03 | 0.06 | 0.07 | 0 | 0.01 | 0.04 | 0 | 0.1 | 0.01 | 0.02 | 0.07 | 0.05 | 0 |
| MgO | 8.8 | 9.93 | 9.48 | 9.73 | 11.23 | 11.54 | 10.56 | 6.92 | 8.55 | 10.23 | 11.47 | 12.13 | 11.33 | 9.32 | 10.29 | 10.46 | 13.15 | 11.1 |
| CaO | 0 | 0 | 0.03 | 0 | 0.03 | 0.01 | 0 | 0.02 | 0 | 0.04 | 0.02 | 0.02 | 0.02 | 0 | 0.12 | 0 | 0.02 | 0.05 |
| BaO | 0.2 | 0.25 | 0.45 | 0.23 | 0.18 | 0.21 | 0.51 | 0 | 0.37 | 0.21 | 0.38 | 0.37 | 0.49 | 0.28 | 0.22 | 0.12 | 0.35 | 0.05 |
| Na2O | 0.45 | 0.12 | 0.35 | 0.17 | 0.23 | 0.36 | 0.18 | 0.11 | 0.32 | 0.12 | 0.36 | 0.22 | 0.22 | 0.15 | 0.1 | 0.05 | 0.12 | 0.16 |
| K2O | 8.88 | 8.94 | 8.34 | 9.24 | 8.85 | 9.06 | 9.33 | 5.29 | 9.26 | 10.22 | 9.6 | 10.13 | 9.65 | 9.5 | 10.6 | 10.53 | 10.61 | 10.32 |
| F | 0.1 | 0 | 0.32 | 0 | 0.13 | 0.55 | 0 | 0 | 0.52 | 0.16 | 0.26 | 0.38 | 0.48 | 0.38 | 0.37 | 0.55 | 0.53 | 0.36 |
| Cl | 0.01 | 0 | 0.16 | 0 | 0.01 | 0.03 | 0.02 | 0.07 | 0 | 0.02 | 0.01 | 0.01 | 0.03 | 0.01 | 0 | 0.01 | 0.01 | 0.03 |
| TOTAL | 94.67 | 92.57 | 93.64 | 93.31 | 93.44 | 95.4 | 94.03 | 90.33 | 94.05 | 95.17 | 94.61 | 95.86 | 94.66 | 94.3 | 95.61 | 95.1 | 95.12 | 95.46 |

| Sample | B2009 | B401 | B428 | B495 | B1139 | B756 | B1433 | B1538 | B1517 | B691 | B618 | B639 | B516 | B1352 | B310 | B281 | B255 | B337 |
|--------|-------|------|------|------|-------|------|-------|-------|-------|------|------|------|------|-------|------|------|------|------|
| | rim | rim | rim | rim | rim | rim | rim | rim | rim | rim | rim | rim | rim | rim | rim | rim | rim | rim |
| SiO2 | 36.19 | 33.98 | 35.09 | 34.57 | 34.88 | 35.23 | 34.46 | 30.61 | 34.62 | 35.09 | 35.43 | 34.78 | 33.35 | 33.86 | 33.77 | | 35.65 | 34.67 |
| Al2O3 | 18.28 | 19.16 | 19.13 | 19.03 | 18.84 | 18.97 | 20.25 | 20.99 | 19.05 | 18.35 | 19.33 | 18.45 | 18.82 | 19.32 | 17.77 | | 16.51 | 18.79 |
| TiO2 | 1.58 | 1.76 | 1.28 | 1.86 | 1.21 | 2.16 | 1.48 | 1.21 | 2.08 | 3.73 | 2.19 | 3.85 | 1.58 | 2.41 | 4.5 | | 4.71 | 4.42 |
| Cr2O3 | 0.16 | 0.07 | 0.22 | 0.1 | 0.08 | 0.13 | 0.09 | 0.03 | 0.21 | 0.08 | 0.08 | 0.19 | 0.1 | 0.06 | 0.07 | 0.18 | | 0.21 |
| FeO | 20.5 | 17.93 | 17.57 | 18.89 | 16.74 | 17.18 | 16.97 | 26.59 | 20.73 | 16.83 | 16.88 | 16.35 | 17.83 | 18.21 | 16.75 | | 12.84 | 14.86 |
| MnO | 0.02 | 0.09 | 0 | 0.15 | 0.02 | 0.07 | 0.14 | 0.03 | 0.12 | 0.01 | 0.05 | 0 | 0.02 | 0 | 0.03 | | 0.08 | 0 |
| MgO | 9.3 | 9.51 | 10.44 | 9.77 | 11.56 | 11.1 | 10.39 | 6.11 | 8.39 | 9.97 | 11.27 | 11.73 | 11.79 | 9.19 | 10.62 | | 13.13 | 11.23 |
| CaO | 0.05 | 0 | 0 | 0 | 0.02 | 0 | 0.06 | 0.04 | 0.02 | 0.03 | 0.03 | 0.01 | 0.01 | 0 | 0.09 | | 0.03 | 0.05 |
| BaO | 0.14 | | | | 0.21 | 0.28 | 0.35 | 0 | 0.27 | 0.16 | 0.38 | 0.37 | 0.23 | 0.03 | 0.09 | | 0.18 | 0.03 |
| Na2O | 0.25 | 0.32 | 0.28 | 0.12 | 0.16 | 0.29 | 0.21 | 0 | 0.29 | 0.11 | 0.38 | 0.19 | 0.22 | 0.1 | 0.1 | | 0.17 | 0.14 |
| K2O | 9 | 9.53 | 9.1 | 9.15 | 9.1 | 9.42 | 8.77 | 4.47 | 9.52 | 10.55 | 9.87 | 9.33 | 9.65 | 9.82 | 10.6 | | 10.5 | 10.34 |
| F | 0.17 | | | | 0 | 0.18 | 0.32 | 0.19 | 0.25 | 0.35 | 0.03 | 0.26 | 0.31 | 0.64 | 0.15 | | 0.87 | 0.1 |
| Cl | 0.02 | | | | 0.02 | 0 | 0.04 | 0.04 | 0.04 | 0 | 0.03 | 0.03 | 0.04 | 0.03 | 0.01 | | 0 | 0.01 |
| TOTAL | 95.66 | 92.35 | 93.11 | 93.64 | 92.84 | 95.01 | 93.53 | 90.31 | 95.59 | 95.26 | 96.06 | 95.45 | 93.91 | 93.72 | 94.66 | | 94.67 | 94.85 |

Compositions expressed as oxides quoted in wt.%. * Electron-microprobe data.

TABLE 4. REPRESENTATIVE COMPOSITIONS* OF PLAGIOCLASE

| sample | P2009 core | P401 core | P428 core | P495 core | P1139 core | P756 core | P1433 core | P1538 core | P1517 core | P691 core | P618 core | P639 core | P516 core | P1352 core | P310 core | P281 core | P255 core | P337 core | P133 core | P131 core | P069 core |
|---|---|---|---|---|---|---|---|---|---|---|---|---|---|---|---|---|---|---|---|---|---|
| SiO2 | 59.82 | 60.26 | 58.86 | 60.71 | 57.73 | 60.15 | 59.15 | 58.65 | 59.67 | 60.14 | 60.45 | 59.56 | 60.82 | 60.89 | 61.59 | 60.16 | 59.1 | 60.8 | 56.3 | 48.71 | 48.47 |
| Al2O3 | 24.91 | 23.68 | 22.64 | 24.07 | 26.21 | 24.78 | 25.69 | 25.19 | 24.45 | 24.46 | 24.02 | 25.13 | 24 | 24.41 | 23.49 | 25.16 | 25.55 | 24.43 | 27.04 | 32.54 | 32.17 |
| Na2O | 7.75 | 8.48 | 9.05 | 8.56 | 7.04 | 7.99 | 8.09 | 8.36 | 9.16 | 8.15 | 8.29 | 7.62 | 8.07 | 9.06 | 8.54 | 7.92 | 7.52 | 8.13 | 6.23 | 2.54 | 2.64 |
| CaO | 6.95 | 5.57 | 4.6 | 5.73 | 8.2 | 6.24 | 6.79 | 6.5 | 5.43 | 6.09 | 6.13 | 6.83 | 6.02 | 5.35 | 5.01 | 6.36 | 7.15 | 6.23 | 8.77 | 15.81 | 15.68 |
| K2O | 0.02 | 0.08 | 0.08 | 0.08 | 0.03 | 0.06 | 0.06 | 0.06 | 0.05 | 0.25 | 0.05 | 0.12 | 0.1 | 0.1 | 0.28 | 0.21 | 0.27 | 0.13 | 0.37 | 0.07 | 0.12 |
| BaO | 0.04 | 0.01 | 0.15 | 0.22 | 0.07 | 0.05 | 0.17 | 0.14 | 0.03 | 0.01 | 0 | 0.1 | 0 | 0 | 0.05 | 0.04 | 0.06 | 0.1 | 0 | 0.13 | 0.03 |
| SrO | 0.05 | 0 | 0 | 0 | 0 | 0 | 0.31 | 0.3 | 0.29 | 0 | 0 | 0 | 0 | 0.36 | 0 | 0 | 0 | 0 | 0 | 0 | 0 |
| FeO | 0.05 | 0.09 | 0.1 | 0.06 | 0.1 | 0.03 | 0.08 | 0.09 | 0.07 | 0 | 0.02 | 0 | 0.02 | 0.03 | 0 | 0.02 | 0.05 | 0.02 | 0.07 | 0.16 | 0.17 |
| TOTAL | 99.59 | 98.17 | 95.48 | 99.42 | 99.38 | 99.3 | 100.34 | 99.29 | 99.15 | 99.1 | 98.96 | 99.36 | 99.03 | 100.2 | 98.96 | 99.87 | 99.7 | 99.84 | 98.78 | 99.96 | 99.28 |
| An | 0.3309 | 0.2652 | 0.2405 | 0.2689 | 0.3909 | 0.3004 | 0.3157 | 0.2995 | 0.246 | 0.2881 | 0.2892 | 0.3289 | 0.2902 | 0.2446 | 0.2408 | 0.3519 | 0.3391 | 0.2952 | 0.4281 | 0.7715 | 0.7611 |
| Ab | 0.668 | 0.7308 | 0.757 | 0.7272 | 0.6074 | 0.6962 | 0.681 | 0.6972 | 0.7513 | 0.6979 | 0.708 | 0.6642 | 0.7041 | 0.7499 | 0.7431 | 0.637 | 0.6456 | 0.6974 | 0.5504 | 0.2244 | 0.232 |
| Or | 0.0011 | 0.004 | 0.0025 | 0.0039 | 0.0017 | 0.0034 | 0.0033 | 0.0033 | 0.0027 | 0.0141 | 0.0028 | 0.0069 | 0.0057 | 0.0054 | 0.016 | 0.0111 | 0.0152 | 0.0073 | 0.0215 | 0.0041 | 0.0069 |

| sample | P2009 rim | P401 rim | P428 rim | P495 rim | P1139 rim | P756 rim | P1433 rim | P1538 rim | P1517 rim | P691 rim | P618 rim | P639 rim | P516 rim | P1352 rim | P310 rim | P281 rim | P255 rim | P337 rim | P133 rim | P131 rim | P069 rim |
|---|---|---|---|---|---|---|---|---|---|---|---|---|---|---|---|---|---|---|---|---|---|
| SiO2 | 61.03 | 61.41 | 60.78 | 61.62 | 56.58 | 60.97 | 58.13 | 57.16 | 59.12 | 59.98 | 60.51 | 59.93 | 60.42 | 60.64 | 61.52 | 58.92 | 58.46 | 60.31 | 56.16 | 49.27 | 49 |
| Al2O3 | 24.31 | 24.18 | 24.14 | 24.85 | 25.09 | 24.64 | 25.67 | 25.72 | 24.7 | 24.36 | 24.59 | 25.02 | 24.37 | 24.86 | 23.85 | 25.36 | 26.04 | 24.21 | 27.51 | 32.17 | 32.3 |
| Na2O | 8.46 | 8.6 | 8.7 | 8.56 | 6.74 | 7.88 | 8.15 | 7.6 | 9.05 | 7.93 | 8.01 | 7.51 | 8.07 | 9.12 | 8.01 | 7.91 | 7.33 | 7.87 | 5.97 | 2.97 | 2.75 |
| CaO | 5.73 | 5.18 | 5.5 | 5.89 | 8.03 | 6.31 | 6.99 | 6.89 | 5.53 | 6.16 | 6.33 | 6.89 | 6.38 | 5.65 | 5.64 | 6.07 | 7.25 | 6.27 | 9.14 | 15.14 | 15.48 |
| K2O | 0.07 | 0.04 | 0.04 | 0.06 | 0.1 | 0.06 | 0.05 | 0.06 | 0.35 | 0.06 | 0.21 | 0.06 | 0.13 | 0.06 | 0.1 | 0.28 | 0.18 | 0.25 | 0.14 | 0.04 | 0.12 |
| BaO | 0.06 | | | | 0.03 | 0 | 0.11 | 0.08 | 0 | 0.14 | 0 | 0.12 | 0.05 | 0 | 0.16 | 0.02 | 0.08 | 0.15 | 0.07 | 0.05 | 0.01 |
| SrO | 0 | | | 0 | 0 | 0.32 | 0.27 | 0.39 | 0 | 0 | 0 | 0 | 0.28 | 0 | 0 | 0 | 0 | 0 | 0 | 0 | 0 |
| FeO | 0.17 | 0.14 | 0.12 | 0.06 | 0.05 | 0.11 | 0.05 | 0.1 | 0.11 | 0.01 | 0 | 0.03 | 0.03 | 0.01 | 0.03 | 0.06 | 0.02 | 0.05 | 0.65 | 0.08 | 0.4 |
| TOTAL | 99.83 | 99.55 | 99.28 | 101.04 | 96.62 | 99.97 | 99.47 | 98.17 | 98.96 | 98.79 | 99.5 | 99.63 | 99.38 | 100.66 | 99.49 | 99.52 | 99.43 | 99 | 99.74 | 99.72 | 100.06 |
| An | 0.2712 | 0.2491 | 0.2583 | 0.2745 | 0.3946 | 0.3056 | 0.3206 | 0.3271 | 0.2515 | 0.2967 | 0.3029 | 0.3338 | 0.3029 | 0.2536 | 0.2755 | 0.2946 | 0.3483 | 0.3031 | 0.4517 | 0.7652 | 0.7514 |
| Ab | 0.7248 | 0.7486 | 0.7395 | 0.7222 | 0.5996 | 0.6909 | 0.6767 | 0.6531 | 0.7452 | 0.6913 | 0.6937 | 0.6587 | 0.6937 | 0.741 | 0.7082 | 0.695 | 0.6374 | 0.6888 | 0.5341 | 0.2324 | 0.2416 |
| Or | 0.0039 | 0.0023 | 0.0022 | 0.0033 | 0.0059 | 0.0035 | 0.0027 | 0.0198 | 0.0032 | 0.012 | 0.0034 | 0.0075 | 0.0034 | 0.0053 | 0.0163 | 0.0104 | 0.0143 | 0.0081 | 0.0141 | 0.0024 | 0.0069 |

Compositions expressed as oxides in wt.%. * Electron-microprobe data.

TABLE 5. REPRESENTATIVE COMPOSITIONS* OF STAUROLITE

| sample | T1139 core | T1433 core | T756 core | T2009 core | T428 core |
|---|---|---|---|---|---|
| $SiO_2$ | 25.37 | 27.31 | 27.23 | 28.46 | 27.82 |
| $Al_2O_3$ | 54.09 | 54.17 | 53.68 | 52.55 | 54.19 |
| $TiO_2$ | 0.49 | 0.51 | 0.69 | 0.54 | 0.24 |
| $Fe_2O_3$ | 0 | 0 | 0 | 0 | 0 |
| $Cr_2O_3$ | 0.03 | 0.04 | 0.1 | 0.07 | 0.07 |
| FeO | 13.36 | 12.32 | 12.23 | 14.42 | 13.01 |
| MnO | 0.09 | 0.24 | 0.09 | 0.16 | 0.24 |
| MgO | 1.65 | 1.61 | 1.62 | 1.65 | 1.3 |
| TOTAL | 95.08 | 96.2 | 95.64 | 98.01 | 97.32 |

Compositions expressed as oxides quoted in wt.%
* Electron-microprobe data.

TABLE 6. REPRESENTATIVE COMPOSITIONS* OF CORDIERITE

| sample | D428 core | D618 core | D639 core | D310 core | D281 core | D337 core |
|---|---|---|---|---|---|---|
| $SiO_2$ | 47.86 | 47.57 | 47.87 | 48.83 | 48.22 | 48.11 |
| $Al_2O_3$ | 32.38 | 32.76 | 33.66 | 33.32 | 33.08 | 33.38 |
| $TiO_2$ | 0.03 | 0.02 | 0 | 0.01 | 0 | 0 |
| $Fe_2O_3$ | | 1.67 | 2.2 | 1.41 | 1.22 | 1.73 |
| MgO | 8.36 | 8.97 | 9.76 | 9.09 | 9.4 | 9.26 |
| FeO | 7.97 | 5.17 | 3.98 | 6.09 | 5.59 | 5.4 |
| MnO | 0.16 | 0.02 | 0.02 | 0.02 | 0 | 0.08 |
| $Na_2O$ | 0.26 | 0.25 | 0.16 | 0.15 | 0.09 | 0.1 |
| CaO | 0.01 | 0.01 | 0.03 | 0.03 | 0.01 | 0.01 |
| $K_2O$ | 0.01 | 0.03 | 0.01 | 0.02 | 0 | 0.01 |
| TOTAL | 97.15 | 96.47 | 97.69 | 98.97 | 97.61 | 98.08 |

Compositions expressed as oxides in wt. %
* Electron-microprobe data.

andalusite in the sillimanite field, is prevented by the absence of sub-sillimanite-grade rocks. Mineral compositions (Tables 2–7) from the peak assemblage (Table 1) yield core P–T estimates (Grt–Bt thermometer; GASP barometer) of 4.6 kbar at 635°C, whereas rims record 3.8 kbar, 565°C (Table 1, Fig. 6). The lack of significant core-to- rim Ca zoning in garnet (Table 2) suggests that the apparent change in pressure may be an effect of declining temperature on the barometer.

Relationships between structural fabrics and metamorphic minerals are best expressed in pelites. The prin-cipal penetrative fabric $S_2$ is defined by the alignment of biotite and sillimanite and is overgrown by randomly oriented sillimanite. $D_1$ deformation may be recorded in trains of aligned inclusions within staurolite and andalusite porphyroblasts. The youngest ($F_3$, $F_4$) map-scale folds have minor macro- or microscopic expression.

Peak metamorphism in the Vizien belt occurred after 2718 Ma, following deposition of the cover sequence, $D_1$ and $D_2$ structural events. It may have coincided

TABLE 7.  REPRESENTATIVE COMPOSITIONS*
OF PYROXENES AND HORNBLENDE

| sample | C069 core | C131 core | O069 core | O133 core | H069 core | H131 core |
|---|---|---|---|---|---|---|
| $SiO_2$ | 50.92 | 49.45 | 49.2 | 48.42 | 40.76 | 41.59 |
| $Al_2O_3$ | 3.19 | 2.13 | 0.69 | 0.9 | 11.86 | 11.46 |
| $Fe_2O_3$ | 0 | 2.97 | 2.81 | 3.37 | 2.3 | 1.18 |
| $TiO_2$ | 0.12 | 0.24 | 0.11 | 0.05 | 0.07 | 0.14 |
| $Cr_2O_3$ | 0.01 | 0.06 | 0.07 | 0.02 | 3.2 | 4.46 |
| MgO | 12.38 | 9.56 | 14.08 | 13.12 | 17.78 | 17.92 |
| FeO | 17.89 | 12.59 | 32.05 | 32.53 | 0.16 | 0.21 |
| MnO | 0.09 | 0.22 | 0.61 | 0.75 | 7.4 | 6.88 |
| CaO | 12.11 | 21.78 | 0.84 | 0.69 | 11.43 | 11.57 |
| $Na_2O$ | 0.23 | 0.32 | 0.03 | 0.08 | 1.36 | 1.33 |
| F | | | | | 1.7 | 0.99 |
| Cl | | | | | 0.17 | 0.19 |
| | | | | | | |
| TOTAL | 96.94 | 99.32 | 100.49 | 99.93 | 98.22 | 97.97 |
| | | | | | | |
| Wo | 27.95 | 48.47 | 1.82 | 1.53 | | |
| En | 39.77 | 29.63 | 43.12 | 41.2 | | |
| Fs | 32.28 | 21.9 | 55.06 | 57.26 | | |
| | | | | | | |
| FeMg | 0.45 | 0.48 | 0.58 | 0.61 | 0.61 | 0.64 |

Compositions expressed as oxides quoted in wt.%
* Electron-microprobe data. .
Symbols: C: clinopyroxene, O: orthopyroxene, H: hornblende.

broadly with emplacement of peraluminous granitic pegmatites, which also postdate $D_2$. However, there is evidence in some isotopic systems for later resetting. Titanite concentrates from several conglomerate clasts show a range of U–Pb ages from 2650 to 2550 Ma (J.K Mortensen, unpubl. data, 1993). At 635°C, metamorphic recrystallization could have produced some lead loss in titanite ($T_c \approx 650$°C; Scott & St-Onge 1995), however, consistent cooling ages would be expected if this were the case. The spread of ages suggests a younger disturbance of variable intensity. Similarly, a 2444 Ma Ar/Ar age for muscovite in a granitic pegmatite that elsewhere contains monazite of 2620–2693 Ma, appears anomalously young with respect to the *ca.* 2.7 Ga metamorphism that occurred at relatively shallow (8 km) levels in the crust. Thus, a younger disturbance appears likely.

*Kogaluc belt*

The Kogaluc belt is one of several narrow belts of amphibolite-facies supracrustal rocks of the Lake Minto domain (Fig. 2). It has a strike length exceeding 100 km, a maximum width of a few kilometers (Percival *et al.* 1995b), and is bordered by granitic massifs generally of 2.78–2.69 Ga (Percival *et al.* 1992, Skulski *et al.* 1996) containing small remnants of high-grade supracrustal rocks (Percival *et al.* 1992, 1995b).

Dominated by sedimentary protoliths, the generally highly strained Kogaluc belt also contains thin calc-alkaline volcanic units including pillowed basaltic andesite, rhyolite and concordant quartz-feldspar porphyry, interpreted as a continent-margin association (Skulski *et al.* 1996). The felsic rocks, with U–Pb zircon ages of 2759 ± 3 and 2760 ± 5 Ma, respectively (Skulski *et al.* 1996), are considered to represent the age of the Kogaluc strata. Where stratigraphic relations are preserved, the volcanic rocks underlie a prominent unit of banded quartz–magnetite iron formation up to 100 m thick, which is associated with quartz-rich arenites and overlain by lithic arenite and greywacke with minor pelite.

The belt is characterized by pervasive north-striking $D_2$ fabrics, including steep $S_2$ foliation and down-dip $L_2$ mineral lineation, with rare and conflicting indications of kinematic sense (Percival *et al.* 1995a, Lin *et al.* 1995); $F_1$ folds are rarely preserved. Folds with "Z" and sheath geometry (Lin *et al.* 1995) have been variably interpreted as part of a progressive $D_2$ sequence (Lin *et al.* 1995), or as a separate $D_3$ event (Chapdelaine *et al.* 1997). A younger set of north-striking brittle-ductile shear zones indicates late dextral strike-slip.

Peak metamorphic minerals define the $D_2$ structures. The $S_2$ foliation is marked by biotite alignment, and the $L_2$ lineation is formed by hornblende in mafic rocks and sillimanite in pelites. Garnet, andalusite and staurolite are wrapped by the $S_2$ fabric, defined by biotite and sillimanite.

Throughout most of the belt, the peak assemblage in pelites is garnet – sillimanite – biotite – plagioclase – quartz. Near its northern extremity, the belt contains pelites with relics of staurolite and andalusite, and one sample contains cordierite with garnet and sillimanite. Three samples from this region provide quantitative P–T estimates. The temperatures derived from the garnet–biotite thermometer range from 660–710°C at GASP barometer pressures of 4.8–6.5 kbar for cores, to 605–660°C, 4.4–5.1 kbar for grain margins. Core and rim conditions estimated from cordierite – garnet – sillimanite – quartz are 705°C, 5.3 kbar, and 660°C, 4.9 kbar, respectively (Table 1). The 760°C temperature estimate for specimen 428 places it above the stability field for muscovite and quartz, in conflict with the presence of these minerals in the rock. It is possible that the coarse, randomly oriented muscovite is of retrograde origin.

*Payne–Qalluviartuuq belt*

Three distinct lithotectonic assemblages are present in the Payne–Qalluviartuuq lakes area (Fig. 2). 1) The Qalluviartuuq sequence is a volcanic-rock-dominated package of pillow basalts, associated gabbro and anorthosite (2833 Ma; Skulski *et al.* 1996) with depleted light rare-earth-element (*LREE*) contents and positive values of $\varepsilon_{Nd}$. The volcanic rocks are cut by andesite dykes, including one dated at 2842 Ma (T. Skulski, unpubl. data), and overlain by a dominantly andesitic
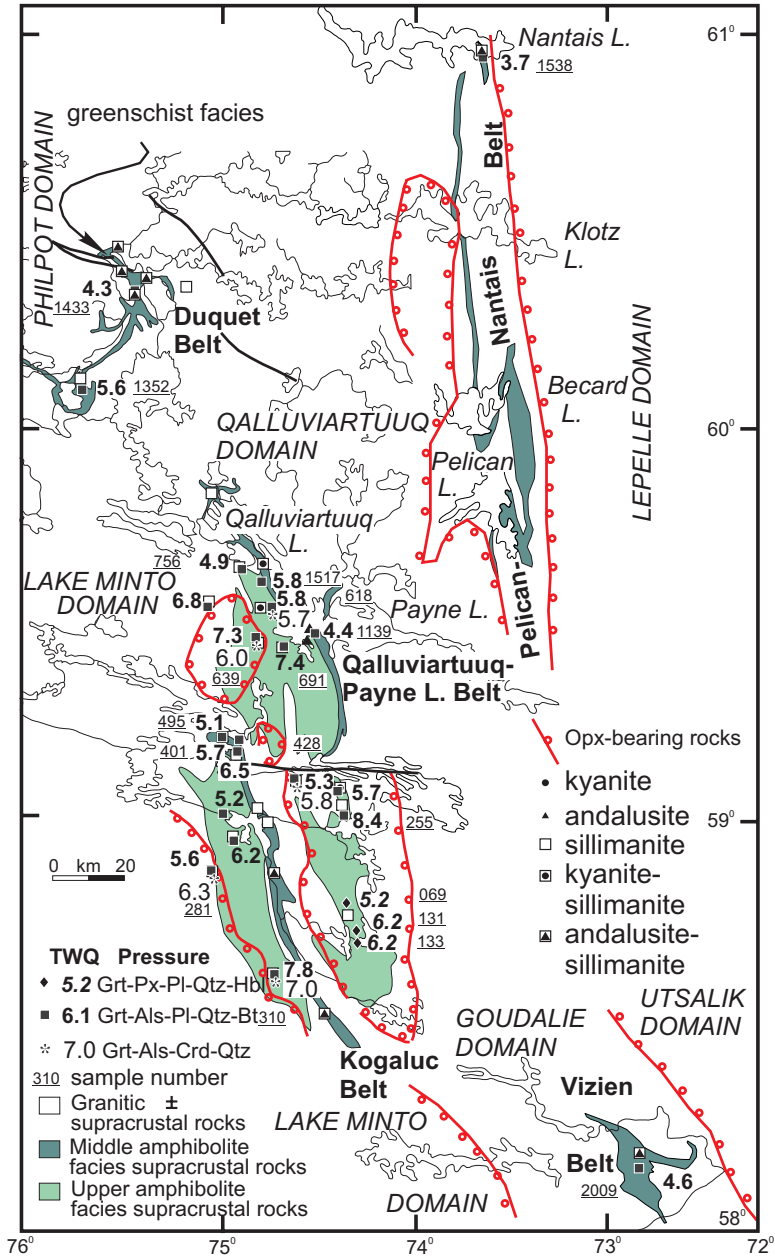
FIG. 6. Regional map showing distribution of maximum recorded pressures in supracrustal units of the Minto block, based on TWQ results from this study (Table 1) and a few additional samples from Stevenson's (1968) collection (Percival & Berman 1996).

volcanic section with diorite and minor peridotite, all characterized by fractionated *REE* patterns and positive values of $\varepsilon_{Nd}$. The supracrustal rocks are cut by a high-level body of granodiorite (2832 Ma; Skulski *et al.*

1996). This assemblage is separated by a tectonic contact from a second, undated sequence (Payne Lake gneisses: Percival *et al.* 1995a) that occurs mainly at high metamorphic grade in Lake Minto domain to its

west. 2) The Payne Lake sequence is dominated by pelitic metasediments, with silicate-facies iron formations, andesites and diorites. Where exposed in the western Payne Lake area, the contact with the Qalluviartuuq sequence is a $D_1$ shear zone overprinted by regional $F_2$ folds and overgrown by middle-amphibolite-facies mineral assemblages. Both the Qalluviartuuq sequence and Payne Lake gneisses are cut by calc-alkaline Hbl – Bt ± Px granodiorites with ages of 2770–2730 Ma (Skulski *et al.* 1996). 3) The third, metasedimentary assemblage occurs sporadically as small, unconformity-bound inliers on units of the Qalluviartuuq sequence and plutons as young as 2775 Ma. It includes basal conglomerate, as well as overlying sandstone, pelite and cordierite–orthoamphibole rocks; a sandstone contains detrital grains of zircon with ages of 2935, 2850, 2836, 2822 and 2748 Ma (T. Skulski, unpubl. data), and conglom-

erates contain granodiorite clasts dated at 2768 Ma (Skulski *et al.* 1996). These rocks and their basement carry a prominent steep $S_2$ foliation and associated down-dip lineation, locally cut by sheets of late syntectonic granite, and warped by open, north-trending $F_3$ folds. Sparse kinematic indicators associated with the $L_2$ stretching lineations suggest west-side-up motion (Percival *et al.* 1995a).

*$D_1$ shear zone boundary*. The boundary between the Qalluviartuuq sequence and Payne Lake gneisses is a 15-m-wide shear zone that can be traced around $F_2$ folds in middle-amphibolite-facies rocks of the western Payne Lake area (Fig. 7). Mafic rocks of the Qalluviartuuq sequence are progressively transformed from pillow basalts to mafic schists over a distance of 5–10 m, and bedded metapelites of the Payne Lake sequence become homogeneous schists adjacent to the contact. The
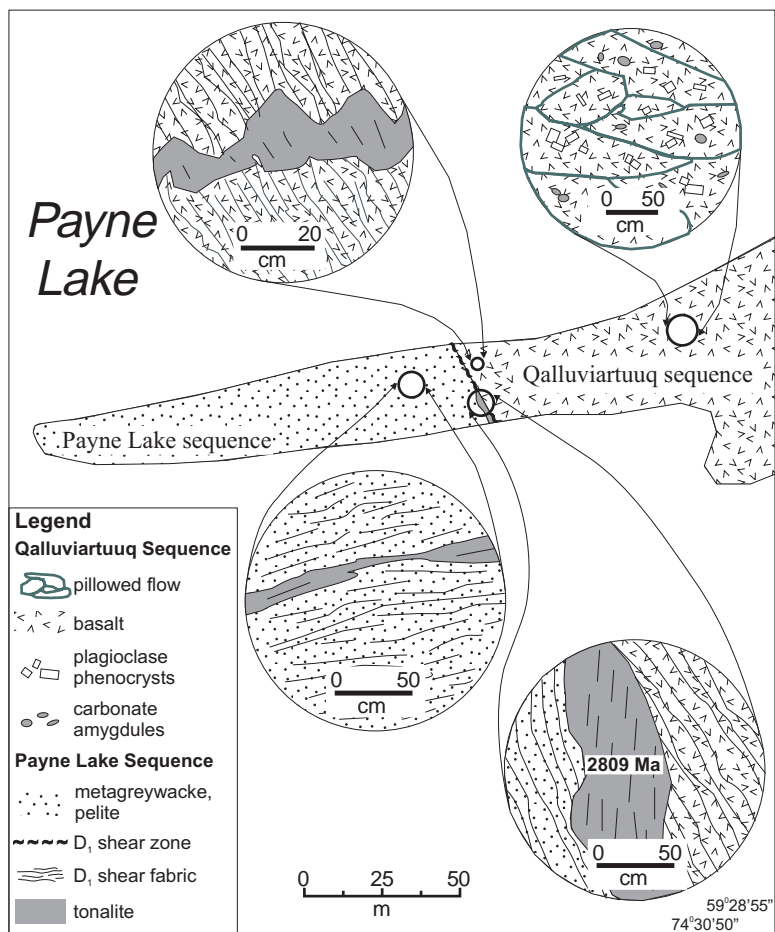


FIG. 7.    Field relationships in the western Payne Lake area. The sketch map shows the Qalluviartuuq and Payne Lake sequences juxtaposed along a $D_1$ shear zone; blowups show details of relationships among the shear zone, tonalite dyke and host rocks.
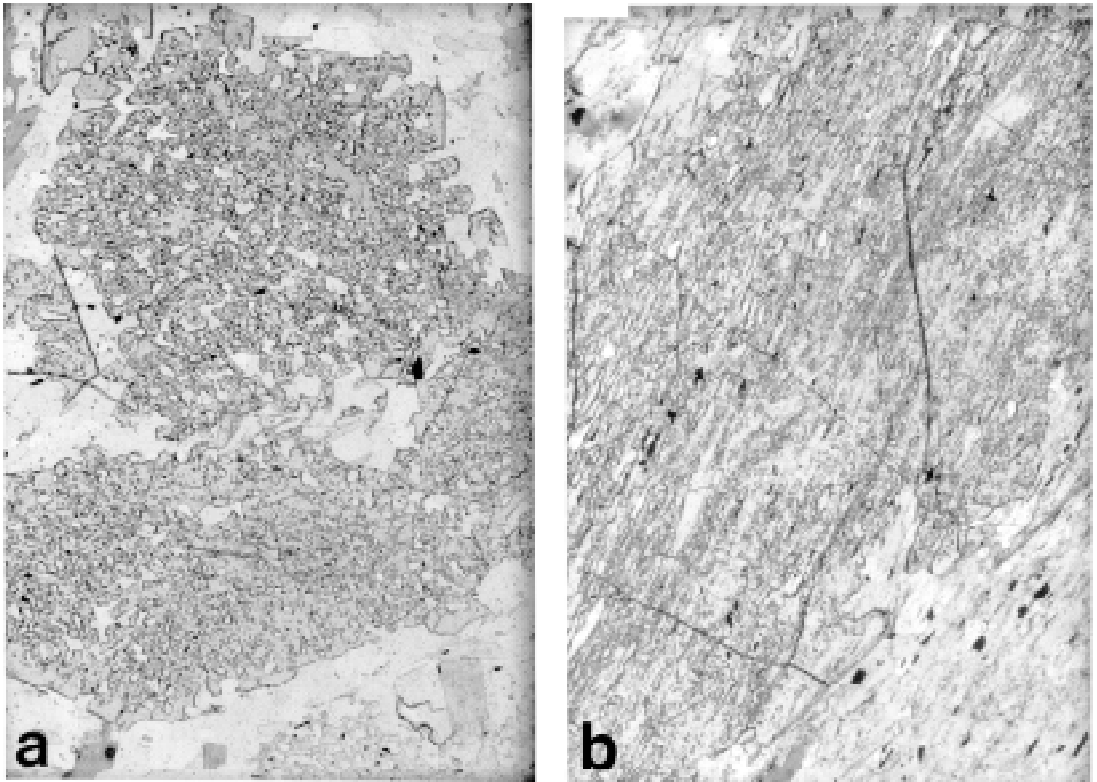
FIG. 8. Photomicrographs of textures illustrating structural-metamorphic relationships in the vicinity of the $D_1$ shear zone: a) staurolite porphyroblasts in schists with preserved bedding contain randomly oriented inclusions of quartz; b) subhedral staurolite porphyroblasts within meters of the shear zone overgrow an intense tectonic fabric.

premetamorphic nature of the shear zone is well illustrated by porphyroblast–matrix relationships (Fig. 8). Where bedding is preserved, staurolite contains randomly oriented inclusions of quartz (Fig. 8a), whereas in the shear zone, staurolite porphyroblasts overgrow a strong tectonic fabric (Fig. 8b). A foliated tonalite dyke occurs within the shear zone and is inferred to be syntectonic on the basis of apophyses of tonalite that cut mafic schists at a high angle but are themselves folded with a weak axial planar foliation concordant to the schistosity in the host. The main body of tonalite carries the characteristic strong foliation and prominent stretching lineation of the host schists (Fig. 8). This dyke was dated to constrain the age of $D_1$ tectonism.

The 2-m-wide tonalite dyke (Fig. 9) yielded three zircon fractions of small, pale, euhedral stubby prisms (single #4, 6a and multigrain #5; sample PBAS96–154, Table 8). These define a U/Pb crystallization age of $2809^{+2}_{-1}$ Ma (Fig. 10) with a MSWD = 0.05 and *ca.* 0 Ma lower intercept. Four zircon fractions (single #1 and multigrain 3a, 3b and 6b, Table 8) of larger prisms and prism fragments have slightly older $^{207}Pb/^{206}Pb$ ages up

to 2814 Ma that reflect small amounts of inheritance (Fig. 10). This date provides a minimum age for the undated Payne Lake supracrustal sequence and coincides with $D_1$ shear-zone deformation. The tectonic significance of this sheared boundary ranges from a minor fault within a coherent Qalluviartuuq – Payne Lake stratigraphic pile, to an important accretionary boundary between two unrelated sequences.

*Younger events in the Payne–Qalluviartuuq region.* Regional middle-amphibolite-facies metamorphism is recorded in all units including the <2748 Ma sedimentary rocks. The lowest-grade rocks occur in western Payne Lake, where staurolite and andalusite porphyroblasts are well preserved, and sillimanite is locally scarce. Two types of andalusite are present in this area: grey, inclusion-riddled porphyroblasts, and pink, inclusion-free rims and discrete grains. The pink andalusite could represent a product of incipient breakdown of staurolite in the andalusite field, which would indicate bathozone 2 of Carmichael (1978) [<3.3 kbar; see discussion in Pattison & Tracy (1991)]. Minerals show significant compositional zoning. A detailed compositional

TABLE 8. U-Pb RESULTS FROM NORTHERN MINTO BLOCK SAMPLES

| Sample[1] | Weight μg | U ppm | Pb$_c$[2] (pg) | $\frac{207Pb[3]}{204Pb}$ | $\frac{Th[4]}{U}$ | $\frac{206Pb[5]}{238U}$ (±1σ) | $\frac{207Pb[5]}{235U}$ (±1σ) | $\frac{207Pb[5]}{206Pb}$ (±1σ) | $\frac{207Pb\ Age[6]}{206Pb}$ Ma (±1σ) | Disc. [7] % |
|---|---|---|---|---|---|---|---|---|---|---|
| **Payne PBAS96-154** | | | | | | | | | | |
| 1 zrn, 1 grain | 3.8 | 80 | 3.9 | 529 | 0.495 | 0.54347±.22 | 14.878±.23 | 0.19855±.04 | 2814.3±1.4 | 0.7 |
| 4 zrn, 1 grain | 2.5 | 76 | 8.4 | 160 | 0.438 | 0.51794±.36 | 14.191±.37 | 0.19871±.08 | 2815.6±2.5 | 5.4 |
| 5 zrn, 1 grain | 5.4 | 33 | 7.5 | 173 | 0.434 | 0.54638±.39 | 14.907±.39 | 0.19788±.08 | 2808.8±2.8 | - 0.1 |
| 3b zrn, 3 grains | 3.6 | 174 | 4.5 | 874 | 0.44 | 0.53915±.09 | 14.771±.10 | 0.19870±.03 | 2815.5±1.0 | 1.6 |
| 3a zrn, 2grains | 3.8 | 146 | 13.3 | 6331 | 0.506 | 0.53976±.09 | 14.781±.10 | 0.19862±.03 | 2814.9±1.0 | 1.4 |
| 6b zrn, 2 grains | 3.8 | 88 | 9.3 | 259 | 0.654 | 0.54587±.11 | 14.962±.13 | 0.19880±.05 | 2816.3±1.8 | 0.4 |
| 6a zrn, 1 grain | 5.6 | 45 | 3.9 | 445 | 0.390 | 0.53997±.12 | 14.743±.13 | 0.19802±.04 | 2809.9±1.4 | 1.2 |
| **PBA95-1064** | | | | | | | | | | |
| 1 zm, 1 grain | 2 | 141 | 7.3 | 230 | 0.521 | 0.49065±.13 | 12.375±.06 | 0.18293±.06 | 2679.6±1.9 | 4.8 |
| 2 zm, 1 grain | 2 | 92 | 11 | 112 | 0.549 | 0.51203±.19 | 12.881±.10 | 0.18245±.10 | 2675.3±3.5 | 0.5 |
| 3 zm, 1 grain | 1.5 | 196 | 9.6 | 176 | 0.495 | 0.17913±.15 | 11.722±.08 | 0.17913±.08 | 2644.8±2.6 | 6.4 |
| **PBA94-516a** | | | | | | | | | | |
| 1 mnz, 1 grain | 5.9 | 6818 | 4.2 | 55929 | 6.93 | 0.51913±.08 | 13.273±.10 | 0.18544±.03 | 2702.1±0.9 | 0.3 |
| 2 mnz, 1 grain | 7.0 | 3732 | 4.3 | 37117 | 7.73 | 0.51916±.08 | 13.267±.10 | 0.18534±.03 | 2701.2±0.3 | 0.3 |
| 3 mnz, 1 grain | 4.3 | 2759 | 2.7 | 25422 | 7.45 | 0.51881±.08 | 13.259±.09 | 0.18535±.03 | 2701.3±0.3 | 0.3 |
| 4 mnz, 1 grain | 3.4 | 977 | 1.8 | 10456 | 8.99 | 0.52035±.08 | 13.325±.09 | 0.18572±.03 | 2704.6±0.3 | 0.2 |
| **PBA94-255** | | | | | | | | | | |
| 1 mnz, 10 grains | 2.1 | 984 | 4.6 | 2635 | 12.6 | 0.51992±.08 | 13.291±.09 | 0.18540±.03 | 2701.8±0.9 | 0.1 |
| 2 rt, 50 grains | 44.8 | 1.4 | 11.1 | 42.0 | 0.0 | 0.46978±.09 | 10.610±.75 | 0.16380±.38 | 2495±12.8 | 0.6 |
| **PBAS96-149** | | | | | | | | | | |
| 1 mnz, 1 grain | 2.9 | 1160 | 14.8 | 24301 | 59.51 | 0.52013±.08 | 13.299±.10 | 0.18544±.03 | 2702.1±0.9 | 0.3 |
| 2 mnz, 1 grain | 16.6 | 1401 | 8.5 | 13431 | 37.55 | 0.52086±.08 | 13.316±.09 | 0.18542±.03 | 2701.9±0.9 | 0.1 |
| 3 mnz, 1 grain | 16.5 | 1699 | 7.0 | 16099 | 25.15 | 0.52025±.08 | 13.301±.10 | 0.18543±.03 | 2702.0±0.9 | 0.0 |
| 4 mnz, 1 grain | 8.2 | 3005 | 6.0 | 23591 | 12.4 | 0.52320±.08 | 13.519±.09 | 0.18741±.03 | 2719.5±0.9 | 0.1 |
| **Pelican-Nantais PBA95-1538** | | | | | | | | | | |
| 1mnz, 4 grains | 4.1 | 1365 | 2.3 | 14224 | 7.33 | 0.51964±.08 | 13.296±.09 | 0.18558±.03 | 2703.4±0.9 | 0.3 |
| 2 mnz, 4 grains | 3.9 | 5698 | 3.3 | 3854 | 7.92 | 0.51908±.08 | 13.276±.09 | 0.18550±.03 | 2702.7±0.9 | 0.3 |
| 3 mnz, 11 grains | 3.4 | 1412 | 2.9 | 9330 | 6.84 | 0.51846±.08 | 13.259±.09 | 0.18548±.03 | 2702.5±0.9 | 0.4 |
| **PBAS96-63A** | | | | | | | | | | |
| 1 ttn, 4 grains | 18.0 | 434 | 575 | 93.7 | 0.475 | 0.51114±.10 | 12.805±.22 | 0.18169±.17 | 2668.4±5.5 | 0.3 |
| 2 ttn, 5 grains | 13.8 | 300 | 45 | 517 | 0.137 | 0.49352±.09 | 12.047±.11 | 0.17714±.04 | 2625.3±1.2 | 1.8 |
| **Vizien PBAS94-274** | | | | | | | | | | |
| 1 mnz, 6 grains | 2.6 | 351 | 17.2 | 308 | 19.02 | 0.50549±.09 | 12.414±.11 | 0.17812±.05 | 2635.4±1.7 | - 0.1 |
| 2 mnz, 10 grains | 3.0 | 1662 | 8.6 | 3186 | 19.33 | 0.50437±.08 | 12.399±.09 | 0.17830±.03 | 2637.1±0.9 | 0.2 |
| 3 mnz, 12 grains | 3.0 | 934 | 5.1 | 2992 | 19.48 | 0.50481±.08 | 12.417±.09 | 0.1784±.03 | 2638.1±0.9 | 0.2 |
| **Kogaluc SNB93-495** | | | | | | | | | | |
| 1 mnz, 4 grains | 3.0 | 1348 | 5.0 | 4346 | 4.99 | 0.50099±.08 | 12.250±.09 | 0.1774±.03 | 2628.2±0.9 | 0.5 |
| 2 mnz, 4 grains | 2.9 | 909 | 7.6 | 1914 | 3.83 | 0.50431±.08 | 12.441±.09 | 0.17892±.03 | 2642.9±0.9 | 0.5 |
| **Duquet PBAS95-1734** | | | | | | | | | | |
| 1 mnz, 5 grains | 4.0 | 412 | 7.1 | 1315 | 7.25 | 0.5083±.09 | 12.698±.10 | 0.18207±.03 | 2671.8±1.0 | 1.5 |
| 2 mnz, 4 grains | 1.0 | 1672 | 7.1 | 1364 | 7.57 | 0.51299±.08 | 12.937±.10 | 0.18291±.03 | 2679.4±1.0 | 0.5 |
| 3 mnz, 1 grain | 2.1 | 307 | 6.6 | 556 | 9.52 | 0.50524±.09 | 12.451±.10 | 0.17873±.03 | 2641.1±1.1 | 0.2 |
| **PBA95-1477** | | | | | | | | | | |
| 1 mnz, 9 grains | 4.0 | 516 | 31.2 | 392 | 12.63 | 0.50666±.03 | 12.539±.10 | 0.17949±.04 | 2648.2±1.4 | 0.3 |
| **PBA94-618** | | | | | | | | | | |
| 1 mnz, 1 grain | 18.4 | 3486 | 9.1 | 40256 | 7.15 | 0.51260±.08 | 12.875±.10 | 0.18216±.03 | 2672.6±0.9 | 0.2 |
| 2 mnz, 1 grain | 8.6 | 2533 | 4.3 | 28474 | 9.60 | 0.51255±.08 | 12.874±.10 | 0.18217±.03 | 2672.7±0.9 | 0.2 |
| 3 mnz, 1 grain | 6.4 | 6442 | 5.0 | 47755 | 3.60 | 0.51567±.08 | 13.070±.10 | 0.18383±.03 | 2687.7±0.9 | 0.3 |
| 4 mnz, 1 grain | 2.5 | 4404 | 4.3 | 14338 | 9.91 | 0.51243±.08 | 12.883±.09 | 0.18234±.03 | 2674.2±0.9 | 0.3 |
| **PBAS95-1461** | | | | | | | | | | |
| 1 ttn, 8 grains | 58.4 | 101 | 73.3 | 501 | 2.22 | 0.53062±.08 | 13.965±.10 | 0.19088±.04 | 2749.8±1.2 | 0.3 |
| **PBAS95-1739** | | | | | | | | | | |
| 1 ttn, 14 grains | 87.0 | 66 | 129 | 300 | 3.62 | 0.5340±.08 | 14.181±.11 | 0.19260±.05 | 2764.5±1.7 | 0.3 |
| **PBAS96-1418** | | | | | | | | | | |
| 1 ttn, 13 grains | 24.1 | 100 | 14.5 | 911 | 0.049 | 0.49692±.09 | 12.005±.10 | 0.17521±.03 | 2608.1±1.1 | 0.4 |
| 2 ttn, 9 grains | 20.4 | 40 | 22.5 | 201 | 0.309 | 0.47496±.13 | 11.462±.14 | 0.17502±.07 | 2606.3±2.4 | 4.7 |
| **PBAS95-1421** | | | | | | | | | | |
| 1 ttn, 8 grains | 36.3 | 93 | 21.3 | 854 | 0.736 | 0.49725±.09 | 12.261±.10 | 0.17883±.04 | 2642±1.2 | 1.8 |
| 2 ttn, 10 grains | 33.8 | 74 | 12.3 | 1110 | 0.092 | 0.50499±.08 | 12.447±.10 | 0.17876±.03 | 2641.4±1.2 | 0.3 |
| **PBAS95-1738** | | | | | | | | | | |
| 1 ttn, 7 grains | 61.6 | 317 | 97.3 | 1140 | 0.391 | 0.49785±.08 | 12.363±.10 | 0.18011±.03 | 2653.9±1.0 | 2.3 |
| 2 ttn, 9 grains | 71.9 | 180 | 98.8 | 789 | 0.394 | 0.51507±.08 | 13.043±.10 | 0.18367±.03 | 2686.2±1.1 | 0.4 |
| **Qalluviartuuq PBAW94-290** | | | | | | | | | | |
| 1 ttn, 15 grains | 53.2 | 48 | 47.1 | 311 | 0.309 | 0.50145±.09 | 12.297±.11 | 0.17785±.05 | 2632.9±1.5 | 0.6 |

[1] mnz: monazite, rt: rutile, ttn: titanite, zm: zircon. [2] Total common lead in analysis corrected for fractionation and spike. [3] Measured ratio corrected for spike and fractionation. [4] Model value based on $^{208}Pb/^{206}Pb$. [5] Corrected for blank and common lead; errors are one standard error of the mean in percent for ratios. [6] Corrected for blank and common lead; errors are two standard errors of the mean in Ma.
[7] Disc% = 100 [ ($^{207}Pb/^{206}Pb$ age) − ($^{206}Pb/^{238}U$ age)] / ($^{207}Pb/^{206}Pb$ age).

Fɪɢ. 9.   Strongly foliated tonalite dyke in the core of the D₁ shear zone, western Payne Lake.
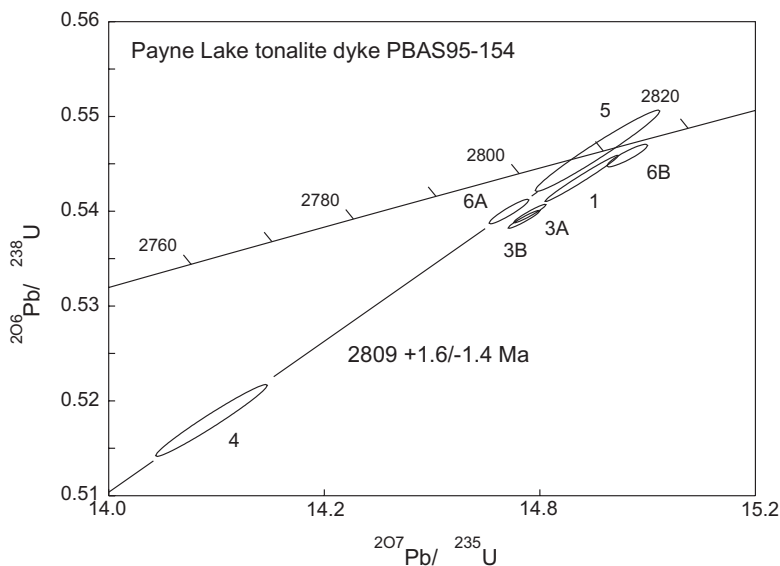


Fɪɢ. 10.   U–Pb concordia diagram showing analyses of zircon grains in syn-D₁ tonalite dyke from the southwest shore of Payne Lake (PBAS–96–154). The U/Pb age of $2809^{+2}_{-1}$ Ma is based on a regression through fractions 4, 5 and 6a.

map of a single grain of garnet in sample 1139 shows a core rich in Mn and Fe, which indicates P–T conditions of 3 kbar, 530°C, in the andalusite field (Table 1, Fig. 5). Rims yield higher values (4.4 kbar, 585°C), consistent with final growth in the sillimanite field. This zonation represents part of a rarely preserved prograde anticlockwise P–T path. Higher P–T conditions are indicated along strike 40 km to the north, where core and rim compositions of minerals in pelite 1517 suggest a decrease from 5.8 kbar, 710°C, to 5 kbar, 630°C.

For the most part, the peak metamorphic assemblages define the prominent $S_2$ foliation and $L_2$ lineation. Constraints on the age of $D_2$ are offered by a body of late syntectonic granite in the northern Qalluviartuuq Lake area. The concordant sheet of granite cuts strongly foliated ($S_2$) mafic schists and carries a weaker, concordant foliation. Apophyses of granite cutting mafic schist are folded, with axial-planar fabric. This body was dated to define the age of late $D_2$ deformation. It contains abundant prismatic zircon and some cores, which were avoided during picking. Regression through a discordant (4.8%) prism tip (#4, PBAS95–1064; Table 8) and a near-concordant, euhedral prism yields a U/Pb crystallization age of $2675^{+4}_{-3}$ Ma (Fig. 11). Fraction 3 is a prism tip that is 6.4% discordant and has a lower $^{207}$Pb/$^{206}$Pb age (2645 Ma), interpreted to reflect complex loss of lead, including ancient and more recent disturbances. The 2675 Ma age is interpreted to mark a late stage of $D_2$ deformation in the Qalluviartuuq belt and also represents a minimum age for the syntectonic metamorphic peak.

The strong $D_2$ fabrics may represent sheared limbs of regional-scale, NW-trending $F_2$ folds developed in the high-grade parts of the region. An east–west crenulation cleavage ($S_4$), present locally in fissile NW-striking zones, probably relates to cross-folds in adjacent high-grade zones.

*Duquet belt*

Two lithological sequences are recognized in the Duquet volcanic-sedimentary belt (Percival *et al.* 1996a, b, 1997a, b): 1) a dominantly basaltic assemblage, and 2) an unconformable sedimentary sequence including iron formation. The older sequence consists primarily of massive and pillowed basalt and gabbro, with plagioclase-phyric andesite and thin sedimentary layers, including greywacke, pelite and silicate-facies iron formation. The calc-alkaline basalts have flat to slightly *LREE*-enriched patterns, with Nd isotopic signatures consistent with some interaction with evolved continental crust. The volcanic rocks are cut by a hypabyssal tonalite pluton dated (U–Pb zircon) at 2775 ± 1 Ma (Percival *et al.* 1996b), coeval with a large pluton of hornblende–biotite granodiorite to the east ($2775^{+5}_{-2}$ Ma; T. Skulski, unpubl. data). To the west, hornblende–biotite granitic rocks of the Philpott domain include tonalitic gneiss (2755 Ma; Percival *et al.* 1997b) and granodiorite (2722 Ma; T. Skulski, unpubl. data).

The younger sequence, which rests unconformably on a 2775 Ma pluton as well as units as old as 2830 Ma (T. Skulski, unpubl. data, 1998), has a lower coarse clastic unit, intermediate amphibolite unit and upper fine clastic unit including pelite, silicate- and oxide-facies iron formations. Deformed conglomerate clasts of 2764
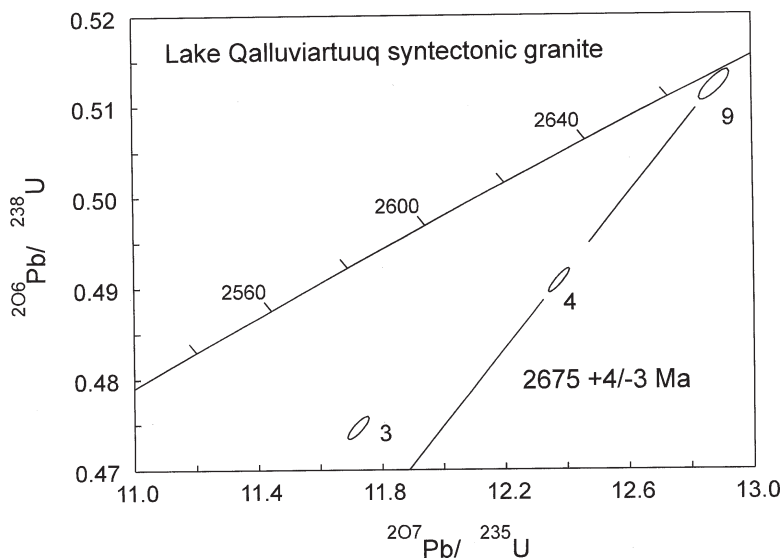


FIG. 11.   U–Pb concordia diagram showing analyses of zircon grains in late syn-$D_2$ granite from north of Qalluviartuuq Lake (PBA–95–1064). The U/Pb age is based on regression through fractions 4 and 9 and yields an upper intercept age of $2675^{+4}_{-3}$ Ma, interpreted as the age of crystallization of the granite.

Ma (T. Skulski, unpubl. data) provide a maximum age of deposition for the sequence. Metamorphic grade varies from greenschist facies in well-preserved slaty rocks in the north, to middle-amphibolite facies throughout most of the belt. The low-grade rocks are characterized by the non-diagnostic mineral assemblages muscovite – biotite – plagioclase – quartz and chlorite – biotite – plagioclase – quartz. For the most part, pelites carry relict staurolite and andalusite in the peak assemblage garnet – sillimanite – biotite – plagioclase – quartz (Table 1). Relict low-grade almandine is preserved locally as inclusions in staurolite. A specimen from the central part of the belt returned core and rim Grt–Bt/GASP estimates of 4.3 kbar, 600°C, declining to 3.3 kbar, 535°C (Table 1, Fig. 5).

The structural chronology of the Duquet belt is complex. Structures of $D_1$ age are recognized only as foliated $(S_1)$ clasts in conglomerate of the younger sequence. An east–west mylonitic $S_2$ fabric is recognized locally and is overprinted by the penetrative regional north-striking $S_3$ foliation including high-strain zones indicating west-over-east movement. The $S_3$ fabrics are overgrown by minerals formed during the peak of metamorphism, which are deformed in narrow, north-striking $D_4$ shear zones. An east–west $S_5$ crenulation cleavage overprints the sheared rocks and forms the dominant axial-planar slaty cleavage in a $F_5$ fold occupied by the lowest-grade rocks.

*Pelican–Nantais belt*

The <2-km-wide by 220 km long Pelican–Nantais belt (Fig. 2) of dominantly mafic rocks is present 75–100 km east of the main chain of supracrustal belts (Percival *et al.* 1997a; Fig. 2) and represents the only preserved belt of supracrustal rocks of Utsalik domain. These fine- to medium-grained amphibolites contain minor lenses and layers of metagreywacke, rhyolite (2742 ± 1 Ma; Percival *et al.* 1997b), quartz–feldspar porphyry and rare pods of peridotite. Metamorphic grade varies from local middle-amphibolite facies (staurolite – andalusite – sillimanite – muscovite) near the northern and southern ends, to granulite facies (orthopyroxene – clinopyroxene – hornblende) near Klotz Lake (Fig. 2). Metasedimentary rocks occur in association with volcanic units and as discrete migmatitic belts up to 3 km wide. Both hornblende–biotite granodiorite (2720 ± 2 Ma; Percival *et al.* 1997b) and pyroxene-bearing granodiorite (2723 Ma; Percival, Stern & Skulski, unpubl. data) occur in proximity to the belt, with pyroxene-bearing plutons more common in the south.

Metamorphic assemblages and migmatitic layering in the supracrustal rocks define a prominent steep, north-striking $S_1$ foliation that is variably expressed in adjacent granitic units. A down-dip mineral and stretching lineation is developed in the hinge regions of tight to isoclinal folds presumed to be of $D_2$ age. An upper bracket on the age of deformation is provided by a sheet of K-feldspar-megacrystic granodiorite (2719 ± 1 Ma; Percival *et al.* 1997b) that carries the $S_1$ foliation and is folded around an $F_2$ closure in the Becard Lake (Fig. 2) area. Deformation in this belt is relatively young (<2719 Ma) with respect to that in belts to the west (>2730 Ma), but is of similar age to that in the Vizien belt (<2718 Ma).

Quantitative metamorphic information is limited to pelite sample 1538 from the northern reaches of the belt in the Nantais Lake area. Porphyroblasts in the staurolite – garnet – andalusite – sillimanite – biotite – muscovite schist are wrapped by the strong foliation in the matrix. Biotite is partly replaced by chlorite on the 5–20 μm scale, and is relatively poor in K (Table 3). Core garnet, plagioclase and altered biotite yield P–T estimates of 2.7 kbar, 530°C, in the andalusite field. Rim compositions indicate higher conditions (3.7 kbar, 550°C), in the sillimanite field, suggesting that the rock records a segment of a prograde anticlockwise P–T path (Fig. 5), although there is considerable uncertainty in the quantitative estimates because of biotite alteration.

UPPER-AMPHIBOLITE-FACIES ROCKS

Supracrustal rocks in the upper amphibolite facies occur on the flanks of the middle-amphibolite-facies belts (Fig. 2). Pelites at this grade consist of the peak metamorphic assemblage garnet – sillimanite – biotite – plagioclase – quartz – granitic leucosome ± cordierite.

The migmatites indicate that temperatures exceeded the water-saturated granodiorite solidus (*ca.* 660°C; Patiño-Douce & Beard 1995) but not equilibria [5] or [6], with estimated temperatures in the 725°C range:

$$\text{biotite} + \text{sillimanite} = \text{garnet} + \text{cordierite} + \text{K-feldspar} + H_2O \qquad [5]$$

$$\text{biotite} + \text{quartz} = \text{orthopyroxene} + \text{K-feldspar} + H_2O \qquad [6].$$

Kyanite occurs sporadically as a relict phase in pelites of the Payne Lake sequence. Its distribution (Fig. 2) parallels the Qalluviartuuq – Payne Lake boundary over 70 km of strike length between Qalluviartuuq Lake and Pavy Lake (Fig. 2). Kyanite occurs as polygonal porphyroblasts overgrown by sillimanite (Fig. 12) and as isolated inclusions in plagioclase. Its significance is discussed further below (see P–T paths).

Peak assemblages provide a range of P–T conditions, broadly intermediate between the middle-amphibolite and granulite facies (Table 1, Fig. 5). Values based on Grt–Bt and GASP core compositions range from 5.6 to 7.4 kbar and 710–820°C. Pressures based on Grt–Crd–Sil–Qtz are similar (5.7–6.0 kbar), although temperatures are lower (675–690°C). P–T estimates for diatexite 516 cannot be explained. This 100-m-wide sill of massive, medium-grained garnet – sillimanite – biotite granodiorite cuts migmatitic paragneiss of the northern

Kogaluc belt. Its compositional similarity to paragneiss suggests derivation from metasedimentary sources and synmetamorphic emplacement. However, core and rim compositions indicate that pressure increased during garnet growth, from 3.3 kbar to within the range of northern Kogaluc pelites, 5.25 kbar; temperatures of 625–630°C are lower than those inferred for the surrounding migmatites (>650°C). These observations are difficult to reconcile with evidence for regional temperatures above those required for garnet homogenization (*ca.* 600°C; Spear 1991) and remain enigmatic. It is possible that fluids evolved during melt crystallization promoted extensive re-equilibration.

### GRANULITE-FACIES REGIONS

High-grade supracrustal rocks are abundant only in Lake Minto domain (Figs. 1, 2), where they occur as narrow (<500 m), elongate (up to 20 km strike-length) screens within granitic massifs made up mainly of granodiorite ranging in age from *ca.* 2770–2700 Ma (Percival *et al.* 1992, Stern *et al.* 1994, Skulski *et al.* 1996). Rock types include mafic gneiss, paragneiss, pelitic migmatite, and both silicate- and oxide-facies iron formation. The affinities of most units are uncertain owing to migmatization and deformation. However, oxide-facies iron formation is a distinctive unit present throughout the western Minto block that could correlate with the young, unconformity-bound sequences of the Kogaluc (<2755 Ma) and Duquet (<2764 Ma) belts. Plutonic rocks as old as 2770 Ma also are present in the eastern Lake Minto domain, suggesting that older components could exist in this region. These could be high-grade equivalents of the Payne Lake sequence. With the exception of the iron formations, the supracrustal units carry a steep $S_1$ migmatitic layering concordant to the enclave margins. In some areas, screens of supracrustal rock, granitic hosts and $S_1$ foliation are folded into prominent, map-scale, north-trending, upright, close to tight, moderately doubly-plunging $F_2$ folds (Percival *et al.* 1995a, b, 1996b, Lin *et al.* 1995). Plunge reversals of $F_2$ hinges can be related to open, upright, east–west-trending $F_4$ folds (Percival *et al.* 1995b).

Peak metamorphic minerals define the $S_1$ foliation in migmatite paleosomes. In metapelites, peak assemblages include garnet – sillimanite – biotite – plagioclase – quartz, garnet – sillimanite – cordierite – biotite – plagioclase – quartz, and garnet – sillimanite – cordierite – K-feldspar – plagioclase – quartz. Psammitic compositions have garnet – orthopyroxene assemblages, mafic gneisses orthopyroxene – clinopyroxene – hornblende – plagioclase ± quartz ± garnet, and silicate-facies iron formations, garnet – orthopyroxene – quartz ± grunerite. The minimum temperature for the granulite facies estimated from these assemblages is 725°C. The presence of garnet – cordierite rather than orthopyroxene – sillimanite limits pressure to <8 kbar.

P–T estimates for pelitic granulites based on core compositions of garnet, biotite and plagioclase fall within the range 5.3–8.4 kbar, 700–840°C, with similar values provided by cordierite-bearing rocks (5.8–7.0 kbar; 690–815°C). Rim compositions yield significantly lower temperatures (560–725°C) and correspondingly lower pressures, indicating substantial retrograde equilibration in some rocks. Core compositions of two orthopyroxene-bearing rocks gave estimates in the range
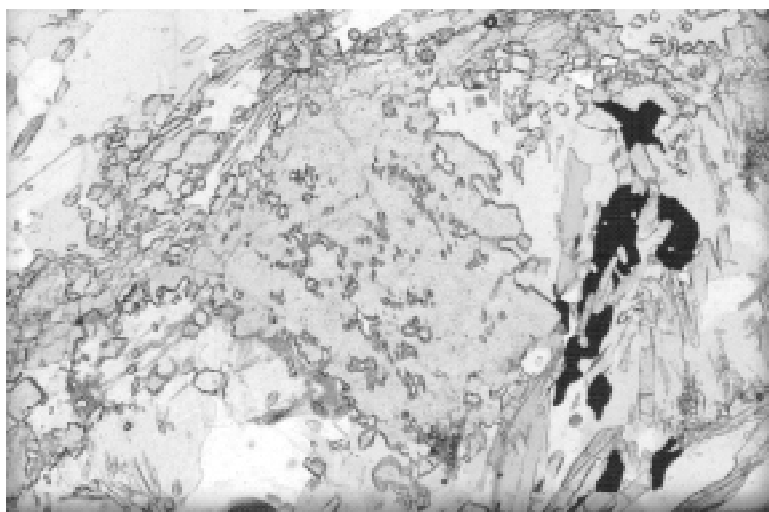


FIG. 12.   Photomicrograph showing polygonal kyanite overgrown by sillimanite in upper-amphibolite-facies pelitic schist. Also present are garnet, biotite, plagioclase and quartz.

5.2–6.2 kbar, 630–730°C using the Fe–Mg Grt–Opx thermometer (Table 1). Even the generally robust Al-in-orthopyroxene thermometer (Aranovich & Berman 1997) yields modest temperatures. These values fall in the retrograde range defined by the pelitic assemblages and may indicate thorough re-equilibration during cooling from high-grade conditions. The degree to which cores also were reset during cooling (*cf.* Pattison & Bégin 1994) is difficult to assess, although temperatures much in excess of 840°C would have produced spinel – quartz instead of the observed garnet – cordierite – sillimanite assemblages.

In the Lake Minto area to the southwest (Figs. 1, 2), spinel and quartz inclusions in cordierite were attributed to peak temperatures locally in the 900–1000°C range (Bégin & Pattison 1994), followed by retrograde growth of cordierite. There, core GASP pressures and Grt–Bt temperatures attained the range 5–6 kbar, 700–800°C, similar to those of pelitic granulites in the present area. Orthopyroxene-bearing assemblages from southern Lake Minto domain give significantly higher estimates of temperature (950–1000°C) using Harley's (1984) Al-in-Opx thermometer. A recalculation of this equilibrium (Aranovich & Berman 1997) yields temperatures only slightly higher than garnet–biotite estimates. Together, these observations suggest that peak temperatures were probably not significantly higher than those recorded by the core compositions.

### SUMMARY OF STRUCTURAL – METAMORPHIC – AGE RELATIONSHIPS

*Relationships among belts of supracrustal rocks, granitic plutons and high-grade equivalents*

Several types of field relationships are evident at contacts between belts of supracrustal rocks and plutonic bodies. In the Vizien belt, the supracrustal rocks are both in unconformable and fault contact with older tonalites of the Goudalie domain; cross-cutting plutonic rocks are restricted to dykes of peraluminous granitic pegmatite. The Goudalie tonalites are transected to the east and west by charnockitic plutons (*ca.* 2725 Ma; Percival *et al.* 1992) of the Utsalik and Lake Minto domains, respectively, which impose contact aureoles on the older rocks (Percival *et al.* 1991, Ross 1991).

To the north, the Kogaluc belt within Lake Minto domain is bounded by variably foliated "wet" plutonic rocks containing amphibolite-facies supracrustal enclaves. These give way east and west to charnockitic plutonic rocks carrying granulite-facies supracrustal enclaves. Peak metamorphic minerals in the Kogaluc belt define a pressure in the interval 4–6 kbar, a strong $S_2$ foliation and down-dip $L_2$ lineations. From field relationships and geobarometry, variable amounts of late synmetamorphic, cross-strike vertical displacement have been accommodated by $S_2$ structures within the Kogaluc belt and its shoulders, possibly shear zones on

limbs of regional folds. At the northern end of the belt, pressures in amphibolite and adjacent higher-grade rocks are similar (*ca.* 6 kbar), whereas to the south, the pressure differential between middle-amphibolite and granulite-facies regions is as large as 3 kbar, implying considerable along-strike structural relief.

Similar relationships are evident at the eastern margin of Lake Minto domain in the Payne Lake area. There, charnockitic plutonic rocks with granulite-facies enclaves grade across strike to the east into "wet" plutons with screens of upper-amphibolite-facies supracrustal rocks, and further east into the middle-amphibolite-facies Qalluviartuuq – Payne Lake belt. The $S_1$ foliation is folded and transposed within this transition. P–T conditions based on minerals defining the $S_2$ fabrics decrease from the range 6.0–7.4 kbar, 700–805°C in high-grade gneisses to 4.4–5.8 kbar, 585–710°C in the amphibolite-facies schists. Some parts of the transition zone show a minor cross-strike pressure differential, whereas as much as a 3 kbar differential exists elsewhere. It is apparent that the variable amounts of vertical offset were accommodated late during metamorphism, along the steep, ductile foliation and lineation, consistent with observations of rare west-side-up kinematic indicators (Percival *et al.* 1995a). The along-strike structural relief within the amphibolite-facies belt cannot be attributed to $F_4$ cross-folds, which would yield sympathetic variations in pressure within the adjacent high-grade regions. Rather, this relief must have developed during formation of earlier structures, and probably reflects plunge variations during $F_2$ folding, such as in the New England Appalachians (*cf.* Kohn *et al.* 1992).

Further north, the Qalluviartuuq and Duquet belts are bordered by "wet" plutonic massifs with sparse supracrustal remnants. Owing to a lack of appropriate assemblages, the metamorphic level of these plutonic domains is unknown, and hence constraints on vertical displacement between greenstones and granites are not available. However, the structural style and chronology in this area are similar to those in areas further south.

Taken together, the association of schistose rocks and low metamorphic grade could support an interpretation that the greenstone belts represent retrograded high-grade rocks. However, several observations conflict with this interpretation: 1) primary sedimentary and volcanic structures are preserved in the amphibolite-facies belts and obliterated by coarse metamorphic minerals at higher grade, 2) assemblages in the lower-grade rocks indicate prograde breakdown of staurolite and andalusite to produce peak-metamorphic garnet and sillimanite, and 3) retrograded migmatitic layering is not present in the amphibolite-facies rocks.

Diapirism has been suggested to be an important mechanism of juxtaposing granites and greenstones in many areas. It is important to note that in the Minto block, upright $F_2$ folds, outlined by supracrustal enclaves, are recognized throughout the granite–granulite

regions. This style of fold is inconsistent with diapiric rise of the granite-dominated massifs. Furthermore, the high-grade regions are characterized by gravity highs, indicating that these regions have higher bulk density than the greenstone belts. As the driving force for diapirism is buoyancy, and the granitic rocks crystallized long before the deformation, the gravity data do not support gravity-driven tectonics.

*Structural – metamorphic – age relationships*

The $D_1$ shear zone bounding the Qalluviartuuq and Payne Lake sequences, dated at 2809 Ma, is premetamorphic with respect to the main low-pressure, high-temperature event. Ages of deposition of the youngest rocks affected by the NNW foliation include <2768 Ma (Duquet belt), <2765 Ma (Qalluviartuuq belt), 2755 Ma (Kogaluc belt), <2748 Ma (Payne Lake belt), 2745 Ma (Pelican–Nantais belt), and <2718 Ma (Vizien belt). Lower bounds on ages of deformation are more difficult to establish owing to the scarcity of cross-cutting plutons and the high uranium contents and discordant nature of their zircon. However, a granitic pegmatite cutting $D_2$ fabrics in the Vizien belt has a monazite age of 2693 Ma, and the late syn-$D_2$ granite in the Qalluviartuuq belt, a zircon age of 2675 Ma.

Available geochronological results support the interpretation of the prominent NNW-striking foliation as an $S_1$ gneissosity in migmatitic rocks, folded and overprinted by regional $D_2$ structures. Subsequent NNW-striking brittle-ductile dextral transcurrent shear-zones are locally developed in the Kogaluc and Duquet belts. Still later, east–west-trending cross-folds and crenulation cleavage represent a regional $D_4$ event. Younger, brittle northwest-trending shear-zones overprint part of the Vizien belt ($D_5$; Lin *et al.* 1995, 1996). The youngest regional structures are zones of pseudotachylite breccia that occupy discordant, WNW-trending aeromagnetic lows. The similar style and orientation of $D_2$–$D_5$ structures, along with their systematic relative chronology from belt to belt, imply a regional extent of these structural events. In the following section, we report U–Pb and other ages that record a spectrum of metamorphic and younger events.

<div align="center">

MONAZITE, TITANITE, RUTILE
AND HORNBLENDE GEOCHRONOLOGY

</div>

*Monazite*

Metamorphic monazite generally begins to crystallize near the staurolite isograd (Smith & Barreiro 1990, Lanzirotti & Hanson 1995, 1997) and is stable throughout the granulite facies (Parrish 1990). Estimates of its closure temperature are in excess of 700°C (Copeland *et al.* 1988, Suzuki *et al.* 1994, Smith & Giletti 1997), and possibly as high as 800°C (Parrish 1990), although it is also subject to lower-temperature recrystallization,

leading to loss of lead and uranium (de Wolf *et al.* 1993, Lanzirotti & Hanson 1995, Hawkins & Bowring 1997, 1999). Monazite has been shown to be a useful chronometer in estimating the age of prograde amphibolite-facies conditions and initial cooling within the granulite facies (Schaltegger *et al.* 1999, Hawkins & Bowring 1999).

Monazite from five rocks in the middle-amphibolite facies, two in the upper-amphibolite facies and two in the granulite facies was analyzed in an attempt to directly constrain the age of regional metamorphism in the Minto block. In the staurolite-bearing schists, monazite occurs as sparse, fine (20–70 µm) subhedral ovoid crystals with abundant quartz and fluid inclusions. The grains have a characteristic patchy surface coating that was not removed in a warm nitric acid bath, and is most likely graphite. Owing to its small size and unknown U content, monazite was generally analyzed as small (3–10 grains) multigrain fractions. Even so, handling was difficult, and several fractions were lost in transfer. In migmatitic rocks and diatexites, the monazite selected for analysis occurs as abundant large (<300 µm), subhedral, inclusion-free crystals, which were run as single-grain fractions. Monazite in the five staurolite-zone samples has variable U contents (307–1672 ppm) and Th/U values (3.8–19.5), whereas that from the high-grade rocks and diatexites has higher U contents (985–6442 ppm U; Table 8).

Four rocks yielded identical U–Pb monazite ages: 2702 ± 2 Ma (Table 8; Figs. 13, 14). These include all of the high-grade and diatexite samples, as well as a sample of staurolite schist from the northern Nantais belt. A previous monazite age of 2704 Ma was reported from the western Utsalik domain (Stern, 1992, Fig. 14). A single-grain fraction from the Pelican diatexite (sample 149) has an age of 2719 Ma and may have been inherited from surrounding units with similar age. More complex results characterize the remaining staurolite-zone rocks, which generally yield a range of monazite ages. Quartzite sample 274 from the Vizien belt has three fractions with indistinguishable ages of 2635, 2637 and 2638 Ma. To the north, sample 495 from the northern Kogaluc belt contains at least two ages of monazite, as multigrain fractions gave 2643 and 2628 Ma. Similarly, in pelite sample 1734 from the Duquet belt, two multigrain fractions gave 2679 and 2672, and a single grain, 2641 Ma. One multigrain fraction from the pelite sample 1477, Payne Lake yielded 2648 Ma. Upper-amphibolite sample 618 gave single-grain ages of 2688, 2673 and 2674 Ma.

*Titanite*

Titanite is a common accessory mineral in calc-alkaline compositions and has a U–Pb closure temperature in the range 660–700°C (Scott & St-Onge 1995). It therefore provides useful constraints on the early cooling history of igneous and metamorphic rocks. Titanite

was extracted and analyzed from several samples of tonalite and granodiorite in the course of the zircon geochronology program (Skulski *et al.* 1996).

A bimodal age population is evident in data for the five rocks presented in Table 8. Two rocks yielded ages near their 2775 Ma age of zircon crystallization (2765, 2748 Ma), significantly older than the age of regional metamorphism. These plutonic rocks (samples 1461, 1739) escaped heating beyond ~650°C during this event. The second age population is younger than the *ca.* 2.7 Ga high-grade event, in the 2686–2606 Ma range. It derives from rocks in low-grade belts (samples 1418, 1421, 1738), as well as one pyroxene-bearing sample (290). Granodiorite sample 1738 has distinct ages for multigrain fractions: 2686 and 2654 Ma. This scattered distribution of ages is difficult to interpret as a regional cooling phenomenon. Rather, it may reflect late, hydrothermal growth or recrystallization of titanite.

### Rutile

A single fraction of rutile was analyzed from pelitic granulite sample 255. This mineral has a closure temperature in the 400°C range (Mezger *et al.* 1989) and thus provides information on the advanced stages of regional cooling. The age of 2495 ± 13 Ma suggests protracted cooling or late hydrothermal growth or resetting. For comparison, rutile in high-grade metamorphic zones of the southwestern Superior Province commonly yields ages younger than that of the meta-

morphic peak by a few tens of million years (Corfu 1988, 1996, Mezger *et al.* 1989).

### Ar/Ar geochronology

Hornblende, with a closure temperature for argon in the 550°C range, was analyzed from three rocks from both low- and high-grade environments, and the results are summarized in Figure 15. The complete dataset is available from the Depository of Unpublished Data, CISTI, National Research Council, Ottawa, Ontario K1A 0S2, Canada. Hornblende from leucogabbro sample QAN92 of the northern Qalluviartuuq belt gave 2569 ± 14 Ma, whereas that from quartz diorite sample 1739 from Lake Ikirtuuq, adjacent to the Duquet belt, is 2643 ± 15 Ma. Mafic granulite sample 132 from the Lake Vernon area, east of the Kogaluc belt, has similar-aged hornblende, at 2641 ± 14 Ma.

### Discussion of geochronological results

A correlation is evident between metamorphic grade and monazite ages (Fig. 13). High-grade rocks and diatexites have homogeneous populations of monazite ages, 2701–2704 Ma, whereas lower-grade rocks have variably younger ages. Exceptions are the staurolite schist from the Nantais belt (2702 Ma monazite) and arenite from the Vizien belt, with a single population of ages (2635–2638 Ma). Three explanations for these patterns of metamorphic ages can be considered: 1) the
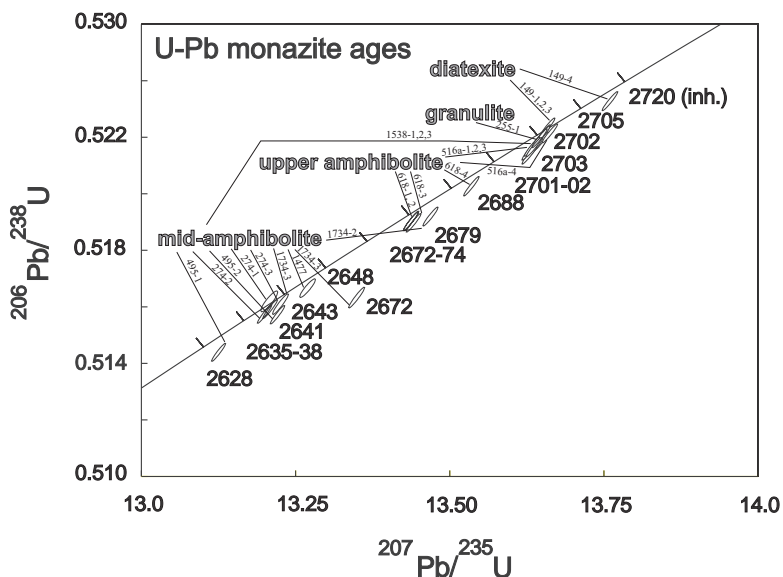


FIG. 13.    U–Pb concordia diagram showing data for monazite from eight rocks.

monazite ages reflect the time of peak prograde meta-morphism. Although the intent of the monazite-dating program was to define metamorphic ages, this interpretation appears unlikely for the greenstone belts for several reasons. First, the age of metamorphism would be different in each belt, and multiple ages from single rocks could not be explained. Second, it is difficult to conceive of a mechanism whereby the lower-grade

belts, which have stratigraphic equivalents at higher grade, could have escaped the effects of the regional high-temperature event at 2702 Ma. It is similarly challenging to postulate a mechanism by which the younger metamorphic events were not recorded in the monazite systematics of the deeper-level rocks. Third, migmatitic paragneisses of the northern Kogaluc belt are cut by massive diatexite with 2702 Ma monazite, providing a
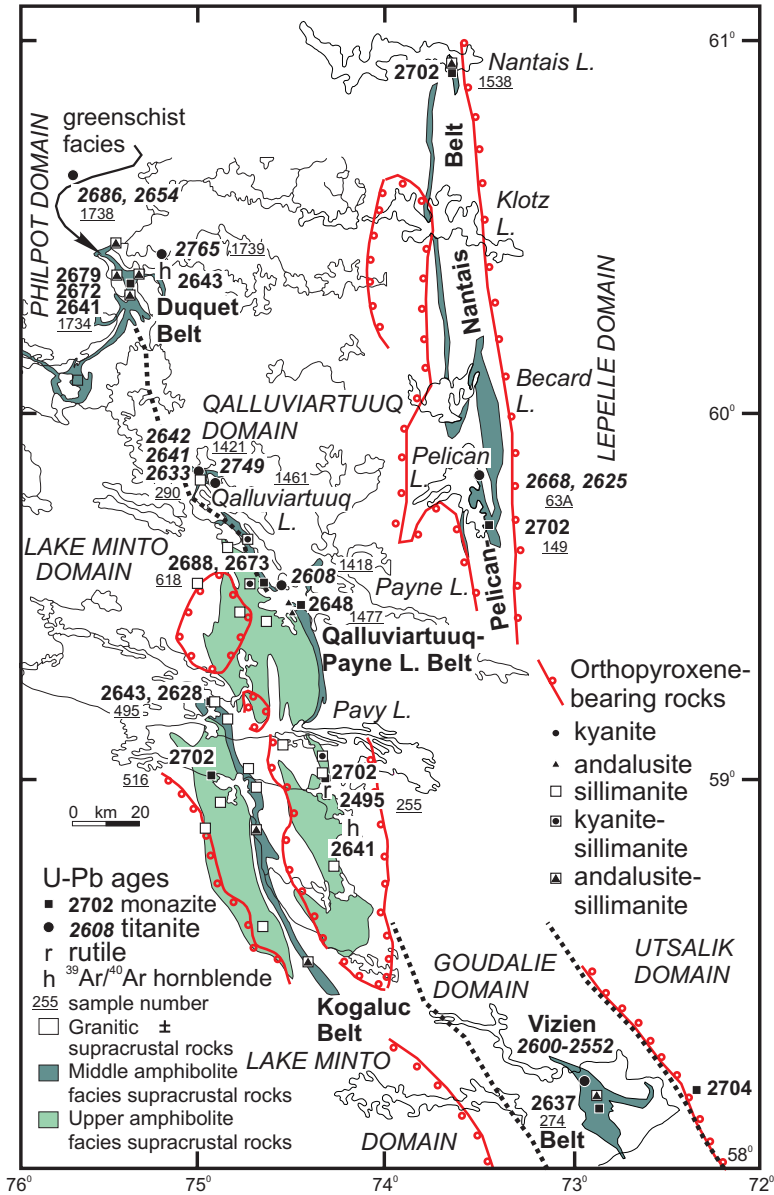


FIG. 14.   Map showing regional distribution of U–Pb monazite, titanite and rutile ages, as well as $^{40}$Ar/$^{39}$Ar plateau ages for hornblende.
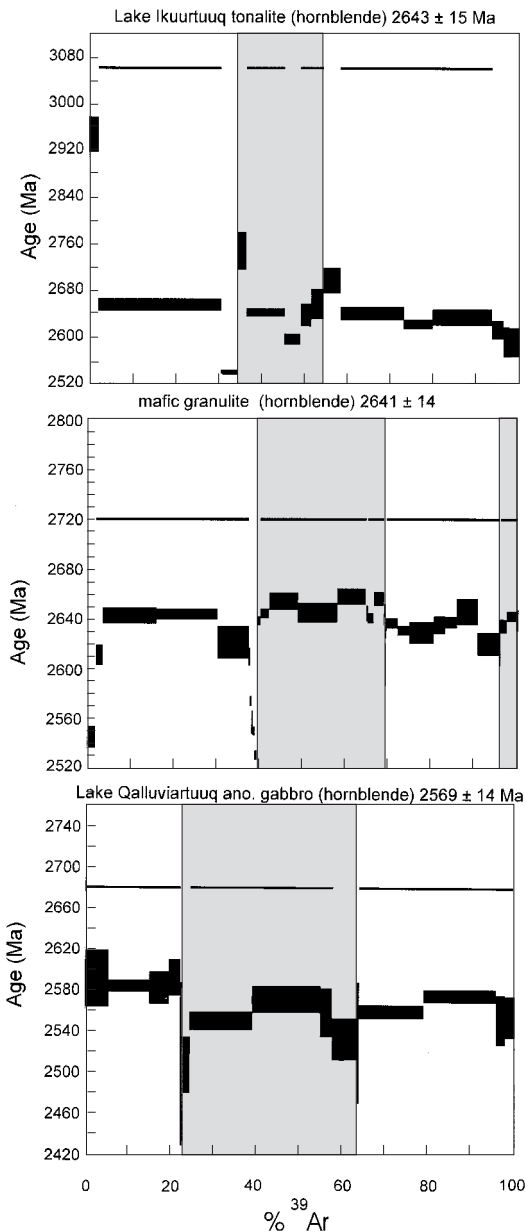
FIG. 15.  Hornblende gas-release spectra for three samples from the Minto block. Alternating backgrounds indicate different aliquots. Steps used in age calculation are indicated by lines with arrowheads. Lake Ikirtuuq tonalite (PBAS–95–1739; zircon U/Pb age of $2775^{+5}_{-2}$ Ma) has a plateau age of 2643 ± 15 Ma. Mafic granulite from high-grade gneisses east of the Kogaluc greenstone belt (PBAS–94–132; likely age is >2725 Ma) has a plateau age of 2641 ± 14 Ma. Qalluviartuuq Lake leucogabbro (QAN92; zircon minimum age of 2832 ± 2 Ma) has a plateau age of 2569 ± 14 Ma. Raw data can be found in the Depository of Unpublished Data (see text).

minimum age for the metamorphism in this part of the belt. Thirty kilometers to the northeast, staurolite-bearing schist sample 495 contains monazite of 2643 and 2628 Ma, yielding a direct contradiction of the hypothesis.

As a second possible explanation, the age of metamorphism is recorded in the homogeneous populations of monazite in the high-grade rocks and diatexites; the younger ages in lower-grade belts reflect late structural events. In terms of relative chronology, the northwest-trending brittle-ductile shear zones and east–west folds and cleavage are post-peak metamorphism, and therefore candidates for new growth of monazite. Simple resetting is unlikely, given the closure temperature of monazite above 700°C and the modest conditions of peak metamorphism in the greenstone belts. This hypothesis does not explain how a second generation of monazite could grow to dominate the population at post-peak temperatures in a closed system (cf. Pan 1997).

As a third possible explanation, the peak of metamorphism was ca. 2702 Ma in both low- and high-grade regions, but late hydrothermal fluids were channeled along permeable structures, and crystallized monazite in structural traps. This interpretation would require that small quantities of monazite grew in the schists during the 2702 Ma event, and that new monazite overgrew old grains or crystallized in new settings at 2645–2628 Ma (cf. Lanzirotti & Hansen 1996, Crowley & Parrish 1999). The multigrain fractions that gave intermediate ages are thus either physical mixtures of these two age components, or contain composite grains (cf. Ayers et al. 1999). The Vizien arenite may not have contained "primary" metamorphic monazite owing to its lack of reactants during the regional metamorphism. Given the small quantities of monazite present in the low-grade pelites and the minor retrogression in most of the rocks, it is unlikely that the proposed hydrothermal event involved large volumes of fluid. Evidence for distinct textural settings for monazite is provided by Duquet pelite sample 1734. Observations in scanning electron microscopy (SEM) show monazite as both inclusions in garnet, biotite and andalusite porphyroblasts, and along grain boundaries (Fig. 16). These may represent examples of synmetamorphic and late growth, respectively. Further resolution of this question would require in situ electron microprobe (cf. Crowley & Ghent 1999, Williams et al. 1999) or SHRIMP (Stern and Sanborn 1998) analyses of potentially complex monazite grains in different structural settings.

## DISCUSSION

### P–T paths

The linear distribution of quantitative P–T points on Figure 5 defines a low-pressure, high-temperature facies series, which is supported by andalusite–sillimanite relationships in middle-amphibolite-facies rocks on the
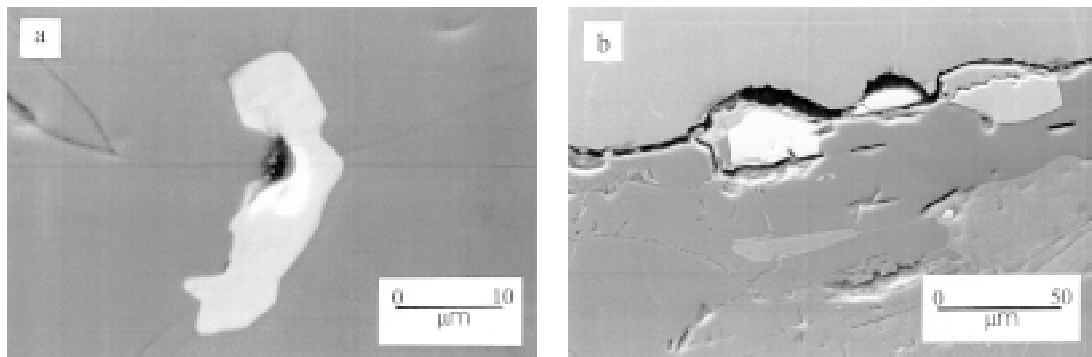
FIG. 16. Textural settings of monazite in Duquet pelite sample 1734. The SEM images show monazite as inclusions in peak-metamorphic minerals such as garnet (a), as well as along grain boundaries (b), suggesting that two ages of monazite growth may be present in the sample.

regional scale. Additional information on the pressure–temperature history of the region can be derived from two datasets: 1) disequilibrium textures preserved in middle- and upper-amphibolite-facies rocks, and 2) chemical zonation in pressure- and temperature-sensitive minerals.

*Aluminosilicates.* The regional distribution of aluminosilicate polymorphs provides an indication of a more complex early metamorphic history than that suggested by the trend on Figure 5. The occurrences of relict kyanite in upper-amphibolite-facies rocks (*e.g.,* Figs. 2, 12) are isolated from the equilibrium assemblage garnet – sillimanite – biotite – plagioclase – quartz that indicates *ca.* 700°C, 5–6 kbar conditions.

Although sporadic, the kyanite occurrences are significant in that they cannot be reconciled with a P–T path that produces an andalusite–sillimanite facies series regionally. Two possibilities can be considered. 1) There may be a polymetamorphic history. A *ca.* 2809 Ma Barrovian metamorphic event, preserved only in rocks older than 2809 Ma and associated with an early collisional event between the Qalluviartuuq and Payne Lake sequences, was overprinted by low-pressure, high-temperature metamorphism at 2702 Ma. Key evidence favoring this hypothesis includes the spatial association between the kyanite occurrences and Qalluviartuuq – Payne Lake boundary, and the absence of kyanite in rocks known to be younger than *ca.* 2760 Ma (Kogaluc belt and correlative rocks in the Duquet belt). In the "polymetamorphic history" hypothesis, the *ca.* 2702 Ma high-temperature event destroyed most of the evidence of the earlier higher-pressure metamorphism. 2) There was a single *ca.* 2.7 Ga regional metamorphic event with regional variations in geothermal gradient. Early kyanite grew in a relatively high P/T regime along the western margin of the >2775 Ma Qalluviartuuq domain, which represented an older, relatively cooler environment than the Lake Minto domain to the west. An underpinning of this hypothesis is the observation of >2748 Ma titanite ages in western Qalluviartuuq domain, which indicate that this area was not heated above ~650°C during the *ca.* 2.7 Ga metamorphism.

Neither hypothesis accounts explicitly for the presence of kyanite in upper amphibolite rocks and its absence in lower-grade rocks. Consideration of the kinetics of kyanite dissolution may offer a possible explanation. Kyanite grains below a certain threshold in size may have recrystallized more readily during the high-temperature phase than larger porphyroblasts, which could have been sufficiently refractory to account for the observed patchy preservation. Similar observations of relict kyanite in high-temperature, low-pressure migmatites of the Quetico belt in the southern Superior Province support this general explanation (Percival 1989, Tabor & Hudleston 1991).

*Paths of chemical zoning*

Single specimens from the Nantais (1538) and Payne (1139) belts show compositional profiles in garnet consistent with preserved growth-induced zoning (Fig. 5). Both have cores rich in Mn and Fe, and a detailed compositional map of a garnet grain in sample 1139 shows concentric zonation and a bell-shaped profile. If we assume that aluminosilicate was present during garnet growth, P–T paths calculated on the basis of compositions of core and rim garnet, biotite and plagioclase suggest moderate core-to-rim increases of pressure and temperature. Both rocks move from the andalusite to sillimanite field (curve of Holdaway 1971), matching textural relationships. The maximum recorded temperatures, 580°C (1139) and 550°C (1538), are consistent with observations from many areas that garnet compositions remain unhomogenized up to temperatures in the 600°C range (Spear 1991). These rare preserved paths are significant in indicating an anticlockwise segment of the prograde P–T trajectory.
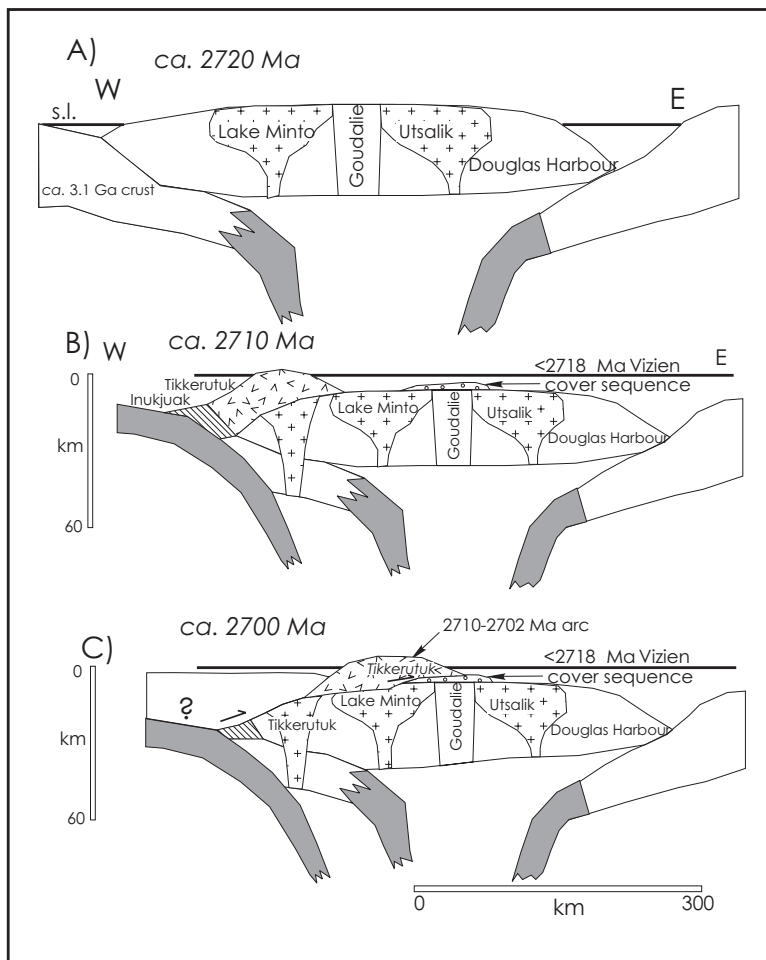
Fig. 17. Schematic tectonic evolution diagram for *ca.* 2.7 Ga tectonothermal events in the Minto block. A) Cessation of 2730–2720 Ma magmatism in the Utsalik and Lake Minto arcs. B) Westward transfer of the locus of magmatism to the Tikkerutuk arc (2710–2702 Ma). C) Eastward thrusting of the hot Tikkerutuk arc superstructure onto the Lake Minto domain, causing burial and rapid heating, followed by thermal relaxation.

The majority of the samples analyzed show compositional zonation typical of retrograde P–T paths. Granulite-facies rocks appear to be most affected, with rim temperatures an average of 100°C lower than those recorded by cores. Temperatures derived from rims in rocks of all grades occupy the 560–720°C range from both garnet–biotite and garnet–cordierite Fe–Mg exchange thermometers. There is unlikely much significance in the lower apparent pressures for the rim, which may simply be attributed to lower-temperature intersections of the GASP equilibrium curve (Bohlen 1987, Frost & Chacko 1989).

Declining temperatures did not produce significant new growth of minerals, such as coronas in granulites

or andalusite in sillimanite schists. This observation could indicate relatively rapid cooling, but conflicts with the evidence for significant retrograde diffusion-controlled re-equilibration in most rocks analyzed. This is a common phenomenon in most high-grade metamorphic terranes, and extended discussion is beyond the scope of this paper.

*Low-P, high-T metamorphism and magmatism*

Plutonic rocks constitute large areas of the Minto block and have a wide spectrum of ages. Given the intimate link between metamorphism and magmatism in many areas (Bohlen 1987, 1991, Clemens 1990,

Lucassen & Franz 1996), it is interesting to consider whether mantle-derived plutonic rocks could have supplied heat for the metamorphism, or whether regional metamorphism caused crustal melting and granite production. In light of the comprehensive geochronological constraints on magmatism and metamorphism in the Minto block, a minimal number of assumptions is required.

Both metamorphic zircon and monazite in high-grade metamorphic rocks and diatexites cluster in the age range 2704–2690 Ma, with monazite ages in lower-grade or altered rocks trailing off to *ca.* 2630 Ma (Table 8, Fig. 13). Older plutonic suites cannot have contributed directly to the metamorphism, although they could have produced high ambient temperatures. In particular, *ca.* 2725 Ma granodiorites represent a widespread plutonic event in the Minto block (Percival *et al.* 1992, 1994, 1998, Stern *et al.* 1994). These large batholithic bodies (Percival & Card 1994) commonly have pyroxene-bearing phases attributed to high-temperature crystallization of $H_2O$-deficient magmas (Percival *et al.* 1992, Stern *et al.* 1994). Evidence supporting an igneous rather than metamorphic origin for the pyroxenes includes: 1) coarse-grained, massive homogeneous textures (Shore 1991; *cf.* Eggins & Hensen 1987), rather than migmatitically layered rocks, 2) the high-temperature assemblage orthopyroxene – clinopyroxene – biotite (*cf.* Naney 1983, Weiss & Troll 1989, Troll & Weiss 1991, Kilpatrick & Ellis 1992) followed in the order of crystallization by hornblende of igneous appearance, 3) geochemical trends indicating increasing fractionation with more hydrous compositions (*cf.* Petersen 1980), and 4) simple morphology and U–Pb systematics of zircon (Percival *et al.* 1992). Apparently, the *ca.* 2700 Ma metamorphism had minor effect on these large bodies of relatively anhydrous character.

Tectonic causes of the low-pressure, high-temperature event may be sought in regional constraints. Observations from the Vizien belt require burial of rocks as young as 2718 Ma to depths of *ca.* 12 km, followed rapidly by the peak of regional high-temperature, low-pressure metamorphism at *ca.* 2700 Ma. Heating to peak temperatures within <20 m.y. is inconsistent with the 30–40 m.y. time scales typical for thermal relaxation following tectonic loading (*cf.* England & Thompson 1984). Rapid transfer of heat could have been accomplished by emplacement of a hot thrust load (Kohn *et al.* 1992), which would have provided an instantaneous thermal pulse (Fig. 17). A probable candidate is the Tikkerutuk arc, the roots of which are exposed west of Lake Minto domain. These granodiorites and granites, with ages of crystallization in the 2710–2704 Ma range (Percival & Card 1994), are autochthonous with respect to the adjacent domains, on the basis of cross-cutting relationships and zircon-inheritance observations. Eastward thrusting of the decapitated arc's superstructure would have led to rapid burial and heating, followed by thermal relaxation that would have produced a second

thermal pulse 30–40 m.y. later. Part of the mainly eroded overthrust block may be preserved in the Vizien belt. There juvenile mafic and ultramafic rocks, which crystallized at 2786 Ma and are interpreted as an oceanic plateau sequence (Skulski *et al.* 1994, Skulski & Percival 1996), were emplaced tectonically on <2718 Ma sediments (Percival *et al.* 1993, Lin *et al.* 1996). These rocks could represent part of the basement on which the Tikkerutuk arc was built.

The hypothesis of a western thrust-load is consistent with the inferred cross-strike geometry of *ca.* 2.7 Ga metamorphic effects in the western Minto block (Fig. 17). On the regional scale, metamorphic pressure and temperature are highest (up to 8 kbar, 850°C) and accompanied by abundant granite and diatexite of 2.7–2.68 Ga (Percival *et al.* 1992, 1998) in granulite-facies rocks of Lake Minto domain. Peak temperature and extent of erosion decline eastward through the amphibolite-facies rocks of the Goudalie and Qalluviartuuq domains. Evidence of 2.7 Ga metamorphism is weak in the Utsalik domain, although appropriate assemblages are sparse.

A second manifestation of the *ca.* 2.7 Ga tectonism included introduction of an ancient crustal component. Stern *et al.* (1994) noted the relatively evolved chemical and Nd isotopic character of 2.70–2.68 Ga diatexites and granites of Lake Minto domain ($^{2.7}\varepsilon_{Nd} = -1$ to $-3$), in contrast to the relatively juvenile nature of its 2725 Ma granodiorites ($^{2.7}\varepsilon_{Nd} = +1.5$ to $+2.5$). These observations suggest the introduction of older, geochemically evolved sources into the western Minto block between 2725 and 2700 Ma. Insight into the nature of the under-thrust crust may be provided by the age of a tonalitic enclave in 2.69 Ga diatexite from Lake Minto domain. This meter-scale gneissic inclusion, presumably derived from a deep source in the crust, has an age of 3125 Ma, with 3500 Ma inheritance (Percival *et al.* 1992), both ages older than any rock dated in the exposed Minto block. In summary, both overthrust and underthrust plates are necessary to explain relationships in the western Minto block, and the overall geometry may resemble the schematic cross-section of Figure 17c.

In the southern Superior Province, a major tectonothermal event at *ca.* 2700 Ma has been recognized in the Wabigoon and Winnipeg River subprovinces. Interpreted as docking of an oceanic Wabigoon and continental Winnipeg River block (Davis & Smith 1990, Corfu & Davis 1992, Corfu 1996), the collision produced widespread deformation and metamorphism to grades ranging from greenschist to granulite facies (Corfu *et al.* 1995). The similarity in age to the 2.7 Ga tectonothermal events in the Minto block may be coincidental, or the two areas could represent segments of a continuous orogenic boundary, although the extrapolation is long beneath Phanerozoic cover. The nature of such a boundary between granite-dominated regions could be difficult to recognize through the screen of younger collisional magmatism.

*Late metamorphic events in Superior Province*

Late to post-metamorphic monazite ages have been observed in several greenstone belts of the southern Superior Province, including Hemlo (Corfu & Muir 1989), Manitouwadge, Winston Lake and Abitibi (Davis *et al.* 1994). Krogh (1993) drew attention to these and other young ages in mineral deposits, particularly gold deposits, in the Superior Province, and proposed a model in which fluids liberated by 2660–2620 Ma metamorphism of the deep crust (8–11 kbar), such as observed in the Kapuskasing structure (Percival & Krogh 1983, Krogh & Moser 1994, Moser *et al.* 1996), were channeled along fault zones and crystallized accessory minerals upon cooling at high (2–4 kbar) structural levels. Although similar deep (8 kbar) and shallow (3–6 kbar) levels are juxtaposed in the Minto block, there is no evidence that the high-grade rocks were metamorphically active at the time of monazite crystallization in the lower-grade belts. Rather, it is apparent from structural-metamorphic relationships that the juxtaposition of structural levels occurred late during the metamorphism. Therefore, the exposed high-grade rocks were not the source of fluids for the 2645–2628 Ma events.

Events in the 2660–2620 Ma range occurred throughout the Superior Province. Some are cryptic, such as the 2630–2660 Ma monazite of the Ashuanipi complex (Percival *et al.* 1992). In addition to monazite ages, Algoman granites (*ca*. 2650 Ma; Heather *et al.* 1996) and granitic pegmatites (2640 Ma; Corkery *et al.* 1992) are widespread, and high-grade metamorphism accompanied by deformation is evident in deep-crust settings, including Kapuskasing and Pikwitonei (Heaman *et al.* 1986). These events are synchronous at the scale of the Superior Province (2000 × 1600 km), implying a process not linked to a margin. Plumes have diameters of appropriate dimension, but generally produce mafic and ultramafic magmas, which are not observed in the Superior Province at this time. Large-scale delamination, in which mantle lithosphere, thickened during final assembly of the Superior Province, became gravitationally unstable, sank and was replaced by hotter asthenosphere, could account for late metamorphism of the deep crust, production of leucogranites, and associated release of hydrothermal fluids. Moser *et al.* (1996) proposed a similar model of delamination, driven by slab roll-back at the southern Superior Province margin, but this is difficult to extend north to the Minto block. Skulski *et al.* (1997) suggested that mantle-derived carbonatite (2660 Ma) and nepheline syenite (2653 Ma) in the Minto block are also related to slab delamination. It may be difficult to distinguish simultaneous slab roll-back at several margins from a process of wholesale delamination.

CONCLUSIONS

The Minto block is a complex orogenic belt formed through a series of 2.8–2.7 Ga tectonomagmatic events, some of which are recognized elsewhere in the Superior Province. The oldest rocks (2.9–3 Ga tonalites) are time-correlative with similar tonalites in the North Caribou Terrane (Thurston *et al.* 1991). Juxtaposition of tholeiitic and calc-alkaline volcanic sequences in the Payne Lake area at 2809 Ma represents an intraoceanic accretion event, was associated with Barrovian metamorphism, and was followed by successor arc magmatism. An arc–rift sequence of conglomerate, greywacke and iron formation, widespread in the western Minto block, was engulfed by widespread continental arc magmatism at 2730–2720 Ma.

Warm ambient crust may have contributed to high-temperature, low-pressure metamorphism during a second orogeny in the western Minto block at *ca*. 2.7 Ga. Rapid burial of rocks as young as 2718 Ma was induced by eastward thrusting of the hot superstructure of the 2710–2704 Ma Tikkerutuk arc, which produced peak conditions at 2.7 Ga, followed by the prolonged effects of thermal relaxation (2690–2660 Ma). An older (>3.1 Ga) continental block may also have been thrust under the western Minto during the same tectonic event. Continued or renewed convergence late in the metamorphism (*ca*. 2675 Ma) produced upright, map-scale $F_2$ folds and shear zones that account for the local preservation of middle-amphibolite-facies rocks. Further structural relief developed during formation of east–west-trending cross-folds, possibly far-field effects of collisional deformation in the southern Superior Province. Greenstone belts acted as channelways for late- to postmetamorphic fluids, resulting in postmetamorphic crystallization of monazite between 2688 and 2628 Ma in low-grade rocks. Post-tectonic activity of this age is common throughout the Superior Province and may reflect large-scale lithosphere delamination.

## REFERENCES

ARANOVICH, L.Y. & BERMAN, R.G. (1997): A new garnet–orthopyroxene thermometer based on reversed $Al_2O_3$ solubility in $FeO–Al_2O_3–SiO_2$ orthopyroxene. *Am. Mineral*. **82**, 345-353.

AYERS, J.C., MILLER, C., GORISCH, B. & MILLEMAN, J. (1999): Textural development of monazite during high-grade metamorphism: hydrothermal growth kinetics, with implications for U,Th–Pb geochronology. *Am. Mineral*. **84**, 1766-1780.

BÉGIN, N.J. & PATTISON, D.R.M. (1994): Metamorphic evolution of granulites in the Minto block, northern Québec: extraction of peak P–T conditions taking account of late Fe–Mg exchange. *J. Metamorph. Geol.* **12**, 411-428.

BERMAN, R.G. (1988): Internally-consistent thermodynamic data for stoichiometric minerals in the system $Na_2O–K_2O–CaO–MgO–FeO–Fe_2O_3–Al_2O_3–SiO_2–TiO_2–H_2O–CO_2$. *J. Petrol.* **29**, 445-522.

_____ (1991): Thermobarometry using multi-equilibrium calculations: a new technique, with petrological applications. *Can. Mineral.* **29**, 833-855.

_____ & ARANOVICH, L.Y. (1996): Optimized standard state and solution properties of minerals. I. Model calibration for olivine, orthopyroxene, cordierite, garnet, and ilmenite in the system $FeO–MgO–CaO–Al_2O_3–TiO_2–SiO_2$. *Contrib. Mineral. Petrol.* **126**, 1-24.

BOHLEN, S.R. (1987): Pressure – temperature – time paths and a tectonic model for the evolution of granulites. *J. Geol.* **95**, 617-632.

_____ (1991): On the formation of granulites. *J. Metamorph. Geol.* **9**, 223-229.

CARD, K.D. (1990): A review of the Superior Province of the Canadian Shield, a product of Archean accretion. *Precamb. Res.* **48**, 99-156.

CARMICHAEL, D.M. (1978): Metamorphic bathozones and bathograds: a measure of the depth of post-metamorphic uplift and erosion on the regional scale. *Am. J. Sci.* **278**, 769-797.

CARRINGTON, D.P. (1995): The relative stability of garnet–cordierite and orthopyroxene – sillimanite – quartz assemblages in metapelitic granulites: experimental data. *Eur. J. Mineral.* **7**, 949-960.

CHAPDELAINE, M., DAIGNEAULT, R., ARCHER, P. & BOUCHARD, M. (1997): Structural controls of gold mineralization in an Archean banded iron formation, Kogaluk property, northeastern Superior Province, Quebec. *Geol. Assoc. Can. – Mineral. Assoc. Can., Program Abstr.* **22**, A25.

CLEMENS, J. (1990): The granulite–granite connexion. *In* Granulites and Crustal Evolution (D. Vielzeuf & P. Vidal, eds.). D. Reidel, Dordrecht, The Netherlands (25-36).

COPELAND, P., PARRISH, R.R. & HARRISON, T.M. (1988): Identification of inherited radiogenic lead in monazite and its implications for U–Pb systematics. *Nature* **333**, 760-763.

CORFU, F. (1988): Differential response of U–Pb systems in coexisting accessory minerals, Winnipeg River Subprovince, Canadian Shield: implications for Archean crustal growth and stabilization. *Contrib. Mineral. Petrol.* **98**, 312-325.

_____ (1993): The evolution of the southern Abitibi greenstone belt in light of precise U–Pb geochronology. *Econ. Geol.* **88**, 1323-1340.

_____ (1996). Multistage zircon and titanite growth and inheritance in an Archean gneiss complex, Winnipeg River Subprovince, Ontario. *Earth Planet. Sci. Lett.* **141**, 175-186.

_____ & DAVIS, D.W. (1992): A U–Pb geochronological framework for the western Superior Province, Ontario. *In* Geology of Ontario (P.C. Thurston, H.R. Williams, R.H. Sutcliffe & G.M. Stott, eds.). *Ont. Geol. Surv., Spec. Vol.* **4**(2), 1335-1346.

_____ & MUIR, T. (1989): The Hemlo – Heron Bay greenstone belt and Hemlo Au–Mo deposit, Superior Province, Ontario, Canada. 2. Timing of metamorphism, alteration and Au mineralization from titanite, rutile, and monazite U–Pb geochronology. *Chem. Geol.* **79**, 201-223.

_____, STOTT, G.M. & BREAKS, F.W. (1995): U–Pb geochronology and evolution of the English River Subprovince, an Archean low P – high T metasedimentary belt in the Superior Province. *Tectonics* **14**, 1220-1233.

CORKERY, M.T., DAVIS, D.W. & LENTON, P.G. (1992): Geochronological constraints on the development of the Cross Lake greenstone belt, northwest Superior Province, Manitoba. *Can. J. Earth Sci.* **29**, 2171-2185.

CROWLEY, J.L. & GHENT, E.D. (1999): An electron microprobe study of the U–Th–Pb systematics of metamorphosed monazite: the role of Pb diffusion versus overgrowth and recrystallization. *Chem. Geol.* **157**, 285-302.

_____ & PARRISH, R.R. (1999): U–Pb isotopic constraints on diachronous metamorphism in the northern Monashee complex, southern Canadian Cordillera. *J. Metamorph. Geol.* **17**, 483-502.

DAVIDSON, A., CARMICHAEL, D.M. & PATTISON, D.R.M. (1990): Field guide to the metamorphism and geodynamics in the southwestern Grenville Province, Ontario. *Int. Geol. Correlation Program, Project* **235/304**, *Field Trip Guide* **1**.

DAVIS, D.W. (1996): Provenance and depositional age constraints on sedimentation in the western Superior transect area from U–Pb ages of zircons. *In* Western Superior Transect, Second Annual Workshop (R.M. Harrap & H. Helmstaedt, eds.). *Lithoprobe Rep.* **53**, 18-23.

_____, PEZZUTTO, F. & OJAKANGAS, R.W. (1990): The age and provenance of metasedimentary rocks in the Quetico subprovince, Ontario, from single zircon analyses: implications for Archean sedimentation and tectonics in the Superior Province. *Earth Planet. Sci. Lett.* **99**, 195-205.

_____, POULSEN, K.H. & KAMO, S.L. (1989): New insights into Archean crustal development from geochronology in the Rainy Lake area, Superior Province, Canada. *J. Geol.* **97**, 379-398.

_____, SCHANDL, E.S. & WASTENEYS, H.A. (1994): U–Pb dating of minerals in alteration halos of Superior Province massive sulphide deposits: syngenesis versus metamorphism. *Contrib. Mineral. Petrol.* **115**, 427-437.

_____ & SMITH, P.M. (1990): Archean gold mineralization in the Wabigoon subprovince, a product of crustal accretion: evidence from U–Pb geochronology in the Lake of the Woods area, Superior Province, Canada. *J. Geol.* **99**, 337-353.

DE WOLF, C.P., BELSHAW, N. & O'NIONS, R.K. (1993): A metamorphic history from micron-scale $^{207}Pb/^{206}Pb$ chronometry of Archean monazite. *Earth Planet. Sci. Lett.* **120**, 207-220.

EGGINS, S. & HENSEN, B.J. (1987): Evolution of mantle-derived, augite–hypersthene granodiorites by crystal–liquid fractionation: Barrington Tops Batholith, eastern Australia. *Lithos* **20**, 295-310.

ENGLAND, P. & THOMPSON, A.B. (1984): Pressure – temperature – time paths of regional metamorphism. I. Heat transfer during the evolution of regions of thickened continental crust. *J. Petrol.* **25**, 894-928.

EVANS, B.W. (1977): Metamorphism of Alpine peridotite and serpentinite. *Annu. Rev. Earth Planet. Sci.* **5**, 397-447.

FROST, B.R. & CHACKO, T. (1989): The granulite uncertainty principle: limitations on thermobarometry in granulites. *J. Geol.* **97**, 435-450.

GOODWIN, A.M. (1996): *Principles of Precambrian Geology*. Academic Press, London, U.K.

HAMILTON, W. (1998): Archean magmatism and deformation. *Int. Geol. Rev.* **40**, 1-33.

HARLEY, S.L. (1984): The solubility of alumina in orthopyroxene coexisting with garnet in FeO–MgO–$Al_2O_3$–$SiO_2$ and CaO–FeO–MgO–$Al_2O_3$–$SiO_2$. *J. Petrol.* **25**, 665-696.

HAWKINS, D.P. & BOWRING, S.A. (1997): U–Pb systematics of monazite and xenotime: case studies from the Paleoproterozoic of the Grand Canyon, Arizona. *Contrib. Mineral. Petrol.* **127**, 87-103.

_____ & _____ (1999): U–Pb monazite, xenotime and titanite geochronological constraints on the prograde to post-peak metamorphic thermal history of Paleoproterozoic migmatites from the Grand Canyon, Arizona. *Contrib. Mineral. Petrol.* **134**, 150-169.

HEAMAN, L.M., MACHADO, N., KROGH, T.E. & WEBER, W. (1986): Preliminary U–Pb zircon results from the Pikwitonei granulite terrain, Manitoba. *Geol. Assoc. Can. – Mineral. Assoc. Can., Program Abstr.* **11**, 79.

HEATHER, K.B., SHORE, G.T. & VAN BREEMEN, O. (1996): Geological investigations in the Swayze greenstone belt, southern Superior Province, Ontario: a final field update. *Curr. Res., Geol. Surv. Can., Pap.* **1996-C**, 125-136.

HENRY, P., STEVENSON, R.K. & GARIÉPY, C. (1998): Late Archean mantle composition and crustal growth in the western Superior Province of Canada: neodymium and lead isotopic evidence from the Wawa, Quetico and Wabigoon subprovinces. *Geochim. Cosmochim. Acta* **62**, 143-157.

HERD, R.K. (1978): Notes on metamorphism in New Quebec. *In* Metamorphism in the Canadian Shield (J.A. Fraser & W.W. Heywood, eds.). *Geol. Surv. Can., Pap.* **78-10**, 78-83.

HOLDAWAY, M.J. (1971): Stability of andalusite and sillimanite and the aluminosilicate phase diagram. *Am. J. Sci.* **271**, 97-131.

KILPATRICK, J.A. & ELLIS, D.J. (1992): C-type magmas: igneous charnockites and their extrusive equivalents. *Trans. R. Soc. Edinburgh* **83**, 155-164.

KOHN, M.J., ORANGE, D.L., SPEAR, F.S., RUMBLE, D., III & HARRISON, T.M. (1992): Pressure, temperature, and structural evolution of west-central New Hampshire: hot thrusts over cold basement. *J. Petrol.* **33**, 521-556.

_____ & SPEAR, F.S. (1991): Error propagation for barometers. 2. Application to rocks. *Am. Mineral.* **76**, 138-147.

KRETZ, R. (1983): Symbols for rock-forming minerals. *Am. Mineral.* **68**, 277-279.

KROGH, T.E. (1982): Improved accuracy of U–Pb ages by the creation of more concordant systems using an air abrasion technique. *Geochim. Cosmochim. Acta* **46**, 637-649.

_____ (1993): High precision U–Pb ages for granulite metamorphism and deformation in the Archean Kapuskasing structural zone, Ontario: implications for structure and development of the lower crust. *Earth Planet. Sci. Lett.* **119**, 1-18.

_____ & MOSER, D.M. (1994): U–Pb zircon and monazite ages from the Kapuskasing uplift: age constraints on deformation within the Ivanhoe Lake fault zone. *Can. J. Earth Sci.* **31**, 1096-1103.

LANZIROTTI, A. & HANSON, G.N. (1995): U–Pb dating of major and accessory minerals formed during metamorphism and deformation of metapelites. *Geochim. Cosmochim. Acta* **59**, 2513-2526.

_____ & _____ (1996): Geochronology and geochemistry of multiple generations of monazite from the Wepawaug Schist, Connecticut, USA: implications for monazite stability in metamorphic rocks. *Contrib. Mineral. Petrol.* **125**, 332-340.

_____ & _____ (1997): An assessment of the utility of staurolite in U–Pb dating of metamorphism. *Contrib. Mineral. Petrol.* **129**, 352-365.

LIN, SHOUFA, PERCIVAL, J.A. & SKULSKI, T. (1996): Structural constraints on the tectonic evolution of a late Archean greenstone belt in the northeastern Superior Province, northern Quebec (Canada). *Tectonophys.* **265**, 151-167.

_____, _____, WINSKY, P., SKULSKI, T. & CARD, K.D. (1995): Strucural evolution of the Vizien and Kogaluc greenstone belts in Minto block, northeastern Superior Province, northern Quebec. *Curr. Res., Geol. Surv. Can., Pap.* **1995-C**, 121-130.

LUCASSEN, F. & FRANZ, G. (1996): Magmatic arc metamorphism: petrology and temperature history of metabasic rocks in the Coastal Cordillera of northern Chile. *J. Metamorph. Geol.* **14**, 249-265.

MACHADO, N., BROOKS, C. & HART, S.R. (1986): Determination of initial $^{87}Sr/^{86}Sr$ and $^{143}Nd/^{144}Nd$ in primary minerals from mafic and ultramafic rocks: experimental procedure and implications for the isotopic characteristics of the Archean mantle under the Abitibi greenstone belt, Canada. *Geochim. Cosmochim. Acta* **50**, 2335-2348.

MENARD, T., CRUDEN, A.R., DAVIS, D. & ROBIN, P.-Y.F. (1997): Himalayan-style metamorphism and tectonics between 2700 and 2650 Ma in the Winnipeg River and Wabigoon subprovinces near Dryden. *In* Western Superior Transect, Second Annual Workshop (R.M. Harrap & H. Helmstaedt, eds.). *Lithoprobe Rep.* **63**, 46-54.

MEZGER, K., HANSON, G.N. & BOHLEN, S.R. (1989): High-precision U–Pb ages of metamorphic rutile: applications to the cooling history of high-grade terranes. *Earth Planet. Sci. Lett.* **96**, 106-118.

MORTENSEN, J.K. (1993): U–Pb geochronology of the eastern Abitibi Subprovince. I. Chibougamau – Matagami – Joutel region. *Can. J. Earth Sci.* **30**, 11-28.

MOSER, D.E. (1994): The geology and structure of the mid-crustal Wawa gneiss domain: a key to understanding tectonic variation with depth and time in the late Archean Abitibi–Wawa orogen. *Can. J. Earth Sci.* **31**, 1064-1080.

_____, HEAMAN, L.M., KROGH, T.E. & HANES, J.A. (1996): Intracrustal extension of an Archean orogen revealed using single-grain U–Pb zircon geochronology. *Tectonics* **15**, 1093-1109.

NANEY, M.T. (1983): Phase equilibria of rock-forming ferromagnesian silicates in granitic systems. *Am. J. Sci.* **283**, 993-1033.

PAN, YUANMING (1997): Zircon- and monazite-forming metamorphic reactions at Manitouwadge, Ontario. *Can. Mineral.* **35**, 105-118.

PARRISH, R.R. (1990): U–Pb dating of monazite and its application to geological problems. *Can. J. Earth Sci.* **27**, 1431-1450.

_____, RODDICK, J.C., LOVERIDGE, W.D. & SULLIVAN, R.W. (1987): Uranium–lead analytical techniques at the Geochronology Laboratory, Geological Survey of Canada. *In* Radiogenic Age and Isotopic Studies, Report 1. *Geol. Surv. Can., Pap.* **87-2**, 3-7.

PATIÑO DOUCE, A.E. & BEARD, J. S. (1995): Dehydration-melting of biotite gneiss and quartz amphibolite from 3 to 15 kbar. *J. Petrol.* **36**, 707-738.

PATTISON, D.R. M. & BÉGIN, N.J., (1994): Zoning patterns in orthopyroxene and garnet in granulites: implications for geothermobarometry. *J. Metamorph. Geol.* **12**, 387-410.

_____ & TRACY, R.J. (1991): Phase equilibria and thermobarometry of metapelites. *In* Contact Metamorphism (D.M. Kerrick, ed.). *Rev. Mineral.* **26**, 105-206.

PERCIVAL, J.A. (1989): A regional perspective of the Quetico metasedimentary belt, Superior Province, Canada. *Can. J. Earth Sci.* **26**, 677-693.

_____ (1991): Granulite-facies metamorphism and crustal magmatism in the Ashuanipi complex, Quebec – Labrador, Canada. *J. Petrol.* **32**, 1261-1297.

_____ (1994): High grade metamorphism. *In* Archean Crustal Evolution (K.C. Condie, ed.). Elsevier, Amsterdam, The Netherlands (35-410).

_____ & BERMAN, R.G. (1996): Minto block: metamorphic-plutonic hinterland in northeastern Superior Province. *Geol. Assoc. Can. – Mineral. Assoc. Can., Program Abstr.* **21**, A74.

_____ & CARD, K.D. (1992): Geology of the Vizien greenstone belt. *Geol. Surv. Can., Open File* **2495** (scale 1:50,000).

_____ & _____ (1994): Geology, Lac Minto – Rivière aux Feuilles, Quebec. *Geol. Surv. Can., Map* **1854A** (scale 1:500,000).

_____, _____ & MORTENSEN, J.K. (1993): Archean unconformity in the Vizien greenstone belt, Ungava Peninsula, Quebec. *Geol. Surv. Can., Pap.* **93-1C**, 319-328.

_____, _____, STERN, R.A. & BÉGIN, N.J. (1990): A geological transect of northeastern Superior Province, Ungava Peninsula, Quebec: the Lake Minto area. *Geol. Surv. Can., Pap.* **90-1C**, 133-141.

_____, _____, _____ & _____ (1991): A geological transect of the Leaf River area, northeastern Superior Province, Ungava Peninsula, Quebec. *Geol. Surv. Can., Pap.* **91-1C**, 55-63.

_____ & KROGH, T.E. (1983): U–Pb zircon geochronology of the Kapuskasing structural zone and vicinity in the Chapleau–Foleyet area, Ontario. *Can. J. Earth Sci.* **20**, 830-843.

_____, MORTENSEN, J.K., STERN, R.A., CARD, K.D. & BÉGIN, N.J. (1992): Giant granulite terranes of northeast-

ern Superior Province: the Ashuanipi complex and Minto block. *Can. J. Earth Sci.* **29**, 2287-2308.

_____ & SKULSKI, T. (1997): Multiple tectonothermal events in the Minto block, northeastern Superior Province, Canada. *Geol. Assoc. Can. – Mineral. Assoc. Can., Program Abstr.* **22**, A115.

_____ & _____ (1998): Tectonic history of the Minto block from 3.1–2.6 Ga. *Geol. Assoc. Can. – Mineral. Assoc. Can., Program Abstr.* **23**, A143-144.

_____, _____, CARD, K.D. & LIN, SHOUFA (1995b): Rivière Kogaluc – Lac Qalluviartuuq region (parts of 34J and 34O), Quebec. *Geol. Surv. Can., Open File Map* **3112** (scale 1:250 000).

_____, _____, LIN, SHOUFA & CARD, K.D. (1995a): Granite–greenstone terranes of the northern Goudalie domain, northeastern Superior Province, Quebec. *Curr. Res., Geol. Surv. Can., Pap.* **1995-C**, 141-150.

_____, _____ & NADEAU, L. (1996a): Granite–greenstone terranes of the northern Minto block, northeastern Superior Province, Quebec. *Curr. Res., Geol. Surv. Can., Pap.* **1996–C**, 157-167.

_____, _____ & _____ (1996b): Geology, Lac Couture, Quebec. *Geol. Surv. Can., Open File Map* **3315** (scale 1:250 000).

_____, _____ & _____ (1997a): Granite–greenstone terranes of the northern Minto block, northeastern Quebec: Pelican–Nantais, Faribault–Leridon and Duquet belts. *Curr. Res., Geol. Surv. Can., Pap.* **1997–C**, 211-221.

_____, _____ & _____ (1997b): Reconnaissance geology of the Pelican–Nantais belt, northeastern Superior Province, Quebec. *Geol. Surv. Can., Open File Map* **3525** (scale 1:250,000).

_____, STERN, R.A. & SKULSKI, T. (1998): Geochronological reconnaissance of the Minto block from SHRIMP II U–Pb zircon studies. *Geol. Assoc. Can. – Mineral. Assoc. Can., Program Abstr.* **23**, A144.

_____, _____, _____, CARD, K.D., MORTENSEN, J.K. & BÉGIN, N.J. (1994): Minto block, Superior Province: missing link in deciphering assembly of the craton at 2.7 Ga. *Geology* **22**, 839- 842.

PETERSEN, J.S. (1980): The zoned Kleivan granite – an end member of the anorthosite suite in southwest Norway. *Lithos* **13**, 79-95.

PILKINGTON, M. & PERCIVAL, J.A. (1999): Crustal magnetization and long-wavelength aeromagnetic anomalies of the Minto block, Quebec. *J. Geophys. Res.* **104**, 7513-7526.

POUCHOU, J.L. & PICHOIR, F. (1984): A new model for quantitative X-ray microanalysis. *La Rech. Aérosp.* **3**, 167-192.

POWELL, W.G., CARMICHAEL, D.M. & HODGSON, C.J. (1995a): Conditions and timing of metamorphism in the southern Abitibi greenstone belt, Quebec. *Can. J. Earth Sci.* **32**, 787-805.

_____, HODGSON, C.J., HANES, J.A., CARMICHAEL, D.M., McBRIDE, S. & FARRAR, E. (1995b): $^{40}$Ar–$^{39}$Ar geochronological evidence for multiple postmetamorphic hydrothermal events focused along faults in the southern Abitibi greenstone belt. *Can. J. Earth Sci.* **32**, 768-786.

RODDICK, J.C. (1983): High precision intercalibration of $^{40}$Ar–$^{39}$Ar standards. *Geochim. Cosmochim. Acta* **47**, 887-898.

_____ (1987): Generalized numerical error analysis with applications to geochronology and thermodynamics. *Geochim. Cosmochim. Acta* **51**, 2129-2135.

_____ (1988): The assessment of errors in $^{40}$Ar/$^{39}$Ar dating. *In* Radiogenic Age and Isotopic Studies; Report 2. *Geol. Surv. Can., Pap.* **88-2**, 3-8.

ROSS, A. (1991): *Geological Interpretation of Reaction Selvages in the Ungava Peninsula, Northern Quebec, Canada.* B.Sc. thesis, Univ. of Alberta, Edmonton, Alberta.

SCHALTEGGER, U., FANNING, C.M., GUNTER, D., MUARIN, J.C., SCHULMANN, K. & GEBAUER, D. (1999): Growth, annealing and recrystallization of zircon and preservation of monazite in high-grade metamorphism: conventional and in-situ U–Pb isotope, cathodoluminescence and microchemical evidence. *Contrib. Mineral. Petrol.* **134**, 186-201.

SCHWARZ, S.H. (1992): *Metamorphism of Cordierite–Anthophyllite and Associated Pelitic Rocks in the Vizien Greenstone Belt, Northeastern Superior Province, Quebec.* B.Sc. thesis, Carleton Univ., Ottawa, Ontario.

SCOTT, D.J. & ST-ONGE, M.R. (1995): Constraints on Pb closure temperature in titanite based on rocks from the Ungava orogen, Canada: implications for U–Pb geochronology and P–T–t path determinations. *Geology* **23**, 1123-1126.

SHORE, G.T. (1991): *On the Nature and Origin of Microgranitoid Enclaves in the Leaf River Area, Ungava Peninsula, Superior Province, Quebec.* B.Sc. thesis, Univ. of Toronto, Toronto, Ontario.

SKULSKI, T., ORR, P. & TAYLOR, B. (1997): Archean carbonatite in the Minto block, NE Superior Province. *Geol. Assoc. Can. – Mineral. Assoc. Can., Program Abstr.* **22**, A138-A139.

_____ & PERCIVAL, J.A. (1996): Allochthonous 2.8 Ga oceanic plateau slivers in a 2.72 Ga continental arc sequence: Vizien greenstone belt, northeastern Superior Province, Canada. *Lithos* **37**, 163-179.

_____, _____ & STERN, R.A. (1994): Oceanic allochthons in an Archean continental margin sequence, Vizien grenstone belt, northern Quebec. *Curr. Res., Geol. Surv. Can., Pap.* **1994–C**, 311-320.

_____, _____ & _____ (1996): Archean crustal evolution in the central Minto block, northern Quebec. *In* Radiogenic Age and Isotopic Studies: Report 9. *Curr. Res., Geol. Surv. Can., Pap.* **1995–F**, 17-31.

_____, STERN, R.A. & CIESIELSKI, A. (1998): Timing and sources of granitoid magmatism, Bienville subprovince, northern Quebec. *Geol. Assoc. Can. – Mineral. Assoc. Can., Program Abstr.* **23**, A174-A175.

SMITH, H.A. & BARREIRO, B. (1990): Monazite U–Pb dating of staurolite grade metamorphism in pelitic schists. *Contrib. Mineral. Petrol.* **105**, 602-615.

_____ & GILLETTI, B. (1997): Lead diffusion in monazite. *Geochim. Cosmochim. Acta* **61**, 1047- 1055.

SPEAR, F.S. (1991): On the interpretation of peak metamorphic temperatures in light of garnet diffusion during cooling. *J. Metamorph. Geol.* **9**, 379-388.

_____ (1993): Metamorphic Phase Equilibria and Pressure – Temperature – Time Paths. *Mineralogical Society of America, Washington, D.C.*

STERN, R.A. (1992): Nd and Sr-isotope studies of monazite, zircon and other minerals in granitoids: examples from northeastern Superior Province, Quebec and Mount Everest, Tibet. *In* Radiogenic Age and Isotopic Studies: Report 5. *Geol. Surv. Can., Pap.* **91-2**, 43-50.

_____, PERCIVAL, J.A. & MORTENSEN, J.K. (1994): Geochemical evolution of the Minto block: a 2.7 Ga continental magmatic arc built on the Superior proto-craton. *Precamb. Res.* **65**, 115-153.

_____ & SANBORN, N. (1998): Monazite U–Pb and Th–Pb geochronology by high-resolution secondary ion mass spectrometry. *Curr. Res.*, *Geol. Surv. Can., Pap.* **1998-F**, 1-18.

STEVENSON, I.M. (1968): A geological reconnaissance of Leaf River map-area, New Quebec and Northwest Territories. *Geol. Surv. Can., Mem.* **356**.

STOTT, G.M. (1997): The Superior Province, Canada. *In* Greenstone Belts (M.J. de Wit & L.D. Ashwal, eds.). Clarendon, Oxford, U.K. (480-507).

SUZUKI, K., ADACHI, M. & KAJIZUKA, I. (1994): Electron microprobe observations of Pb diffusion in metamorphosed detrital monazites. *Earth Planet. Sci. Lett.* **128**, 391-405.

TABOR, J.R. & HUDLESTON, P.J. (1991): Deformation at an Archean subprovince boundary, northern Minnesota. *Can. J. Earth Sci.* **28**, 292-307.

THURSTON, P.C. & CHIVERS, K.M. (1990): Secular variation in greenstone sequence development emphasising Superior Province, Canada. *Precamb. Res.* **46**, 21-58.

_____, OSMANI, I.A. & STONE, D. (1991): Northwestern Superior Province: review and terrane analysis. *In* Geology of Ontario (P.C. Thurston, H.R. Williams, R.H. Sutcliffe & G.M. Stott, eds.). *Ont. Geol. Surv., Spec. Vol.* **4**(1), 81-142.

TROLL, G. & WEISS, S. (1991): Structure, petrography and emplacement of plutonic rocks. *In* Equilibrium and Kinetics in Contact Metamorphism: the Ballachulish Igneous Complex and its Aureole (G. Voll, J. Töpel, D.R.M. Pattison & F. Seifert, eds.). Springer-Verlag, Heidelberg, Germany (39-66).

VILLENEUVE, M.E. & MACINTYRE, D. (1997): Laser $^{40}Ar/^{39}Ar$ ages of the Babine porphyries and Newman Volcanics, Fulton Lake map area, west-central British Columbia. *In* Radiogenic Age and Isotopic Studies; Report 10. *Curr. Res., Geol. Surv. Can., Pap.* **1997-F**, 131-139.

WEISS, S. & TROLL, G. (1989): The Ballachulish Igneous Complex, Scotland: petrography, mineral chemistry, and order of crystallization in the monzodiorite – quartz diorite suite and in the granite. *J. Petrol.* **30**, 1069-1115.

WILLIAMS, H.R., STOTT, G.M., THURSTON, P.C., SUTCLIFFE, R.H., BENNETT, G., EASTON, R.M. & ARMSTRONG, D.K. (1992): Tectonic evolution of Ontario: summary and synthesis. *In* Geology of Ontario (P.C. Thurston, H.R. Williams, R.H. Sutcliffe & G.M. Stott, eds.). *Ont. Geol. Surv., Spec. Vol.* **4**(2), 1255-1332.

WILLIAMS, M.L, JERCINOVIC, M.J. & TERRY, M.P. (1999): Age mapping and dating of monazite on the electron microprobe: deconvoluting multistage tectonic histories. *Geology* **27**, 1023-1026.

YORK, D. (1969): Least squares fitting of a straight line with correlated errors. *Earth Planet. Sci. Lett.* **5**, 320-324.